To the Graduate Council:

I am submitting herewith a dissertation written by Nicolaas Aaldert van Goor entitled "Control of Chaotic and Nonlinear Systems Influenced by Dynamic Noise." I have exmined the final copy of this dissertation for form and content and recommend that it be accepted in partial fulfillment of the requirements for the degree of Doctor of Philosophy, with a major in Chemical Engineering.

Duane D. Bruns

Duane D. Bruns, Major Professor

We have read this dissertation and recommend its acceptance:

Charles F. Moore

C. Stuart Daw

Accepted for the Council:

Associate Vice Chancellor and Dean of the Graduate School

# Control of Chaotic and Nonlinear Systems Influenced by Dynamic Noise

A Dissertation
Presented for the
Doctor of Philosophy
Degree
The University of Tennessee, Knoxville

Nicolaas Aaldert van Goor
August 1998

# Acknowledgements

The completion of my degree would have been impossible without the support of many people. I am very grateful to them all, and hope that I can prove their investment worthy. Though I cannot possibly mention them all here, I would like to single out a few of them that I am particularly grateful to.

The people who had the most influence on my work were, of course, the members of my Dissertation Committee, Duane Bruns, Stuart Daw, Celso Grebogi, Bill Lawkins, Charlie Moore, and Ke Nguyen. Their guidance and encouragement contributed greatly to this dissertation, and I am very grateful to them for their support.

I would also like to express my appreciation for the faculty and staff of the Department of Chemical Engineering. They have supported me, on professional, as well as, friendship levels. I would like to thank the Measurement and Control Engineering Center for its generous financial support, and its members for their support and advice.

Lastly, I owe a great debt of gratitude to my family, my surrogate family, and all of my friends. Without them, none of this would have been possible.

# Abstract

In this research, the effect of dynamic noise on OGY type control algorithms was studied. The research was done by conducting numerical experiments on a number of systems, i.e., the Hénon map, the Ikeda map, a model for internal combustion engines, and a model for continuous stirred tank reactors.

It was found that the fixed point location does not appear to be influenced by Gaussian noise. The manifold structure, however, does change with different noise intensities. Studies were also done to evaluate the effect of noise on directions of maximum and minimum contraction. These were found to be independent of Gaussian noise.

The original OGY control was found to be less that optimal when noise is added to the system. Comparisons were also made between the original OGY and a control algorithm based on the singular value decomposition. The SVD method appeared slightly more robust in noisy environments.

It was found that neither the original OGY, nor the SVD method were optimally suited for control when the system is being influenced by parametric noise. A number of guidelines were proposed and tested to optimize the search for the optimal control condition.

# Contents

# List of Figures

# List of Tables

# Chapter 1

# Background and Objective

## 1.1 Introduction

The earliest recognition that nonlinear systems may exhibit sensitive dependence on initial conditions is attributed to Henri Poincaré, who was studying the "three-body" problem about 100 years ago to determine whether the solar system is stable. The story goes that the king of Sweden offered a prize to whomever could prove that the solar system was stable. Poincaré in fact proved the opposite, but was persuaded by an unhappy king to "revise" his calculations and proclaim that the system was stable. In *The Foundation of Science: Science and Method* (1921), Poincaré writes:

> It may happen that small differences in the initial conditions produce very great ones in the final phenomena. A small error in the former will produce an enormous error in the latter. Prediction

becomes impossible.

Though the concept of sensitivity to initial conditions — which is a hallmark of chaos — was remembered by theoretical mathematicians, it was largely forgotten by physicist and engineers. The computing power to study nonlinear systems was simply not available, and scientists were conditioned to thinking only in linear terms. It was not until 1963 that Lorenz rediscovered this phenomenon when studying a model for global weather patterns using a digital computer. From Lorenz's initial observations, the idea of unpredictable determinism continued to grow until it culminated in the ideas of "chaos theory" in the 1980s.

One major contribution to the expansion of this new field was a paper published by Ott, Grebogi, and Yorke (1990), in which they contradict earlier preconceptions and show a method for controlling chaotic dynamics[1]. This insight sparked the interest of many researchers, and subsequently many papers concerning control of chaotic systems were published. The OGY-method has now been extended to be applicable to a larger variety of systems, and a number of other control methods have been shown to work in principle.

Though "chaos" is now widely accepted and recognized in the academic world as a dominant feature in nature, it remains virtually unused as an industrial tool. One main reason why "chaos theory" has remained largely an academic curiosity is that the theory has so far been applied primarily

[1]This control method is now often dubbed the "OGY-method".

to ideal systems and models. Chaos control methods, for example, work very well on computer models and in laboratory experiments (e.g., Singer, Wang, and Bau (1991), In, Ditto, and Spano (1995), and Parmananda, Shepard, Rollins, and Dewald (1993)). The environments of these experiments, however, are far more controllable and predictable than most engineering systems. In real world applications noise affects the behavior in complex ways. It is precisely because of the nonlinear sensitivity of chaotic systems that these small disturbances have such an important impact. As shown by various authors (e.g., Hamm, Tél, and Graham (1994)), the results of these disturbances can be quite unpredictable and dramatic. The amount of research done to examine the effect of noise (especially *dynamic noise*) has been relatively sparse, though a number of authors have addressed the issue (e.g., Mayer-Kress and Haken (1981), and Wackerbauer (1995)).

## 1.2 Chaos basics

### 1.2.1 Defining chaos

Even after 30 years of collaborative research, there is no universally accepted definition of what a chaotic system is. Ott (1993) states

> We define the attractor to be *chaotic* if it has a positive Lyapunov exponent.

This means that any *attractor*[2] displaying sensitive dependence on initial conditions is considered chaotic. Strogatz (1994), on the other hand, adds some other restrictions:

> Chaos is *aperiodic long-term behavior* in a *deterministic* system that exhibits *sensitive dependence on initial conditions.*

This definition adds the requirement that the system has no stochastic inputs. Later, it will be seen that adding stochastic inputs to a nonlinear system can result in a non-chaotic system becoming sensitive to initial conditions. A question that arises is whether or not this means that the system has become chaotic. The answer would be "yes" according to the first definition, but "no" according to the second. Currently, this phenomenon has been called "noise induced chaos". From a practical point of view, it is important to note that whatever we call the behavior, noisy nonlinear systems are a constant fact of life for most engineers.

### 1.2.2 Dynamic systems

The systems considered here are all dynamic, i.e., "relating to an object, or objects, in motion" (Neufelt 1994). This means the systems are changing in

[2] Ott defines attractors as "bounded subsets to which regions of initial conditions of nonzero phase space volume asymptote as time increases".

time. The equations of motion can be written in general

$$\dot{\mathbf{x}} = \mathbf{F}(\mathbf{x}, \mathbf{p}, t) \tag{1.1}$$

for continuous systems, and

$$\mathbf{x}_{n+1} = \mathbf{F}(\mathbf{x}_n, \mathbf{p}, n) \tag{1.2}$$

for discrete systems. In these equations we have $\mathbf{x} \in \mathbb{R}^N$, which are the state variables, $\mathbf{p} \in \mathbb{R}^{N_p}$, which are the system parameters, and $\mathbf{f}()$, which are a set of $N$ equations describing the behavior. In the following background discussion, only continuous systems will be discussed, since discrete systems follow analogously, unless noted otherwise.

System (1.1) can usually not be solved analytically, and is instead mostly solved using numerical integration algorithms. The solution to (1.1) moves in an $N$-dimensional space called *phase space* (also known as *state space*). The basis of this space is given by the state variables $\mathbf{x}$, i.e., the location of the state of the system is determined by taking all the state variables as orthogonal coordinates in the phase space. The system starts out at a certain *initial condition* $\mathbf{x}_0 = \mathbf{x}(t = 0)$ in the space. From the initial condition, the system evolves over time, tracing a *trajectory* through the phase space, as shown in figure 1.1. The shape in phase space that the trajectory approaches as $t$ reaches infinity is called the *attractor* of the system.

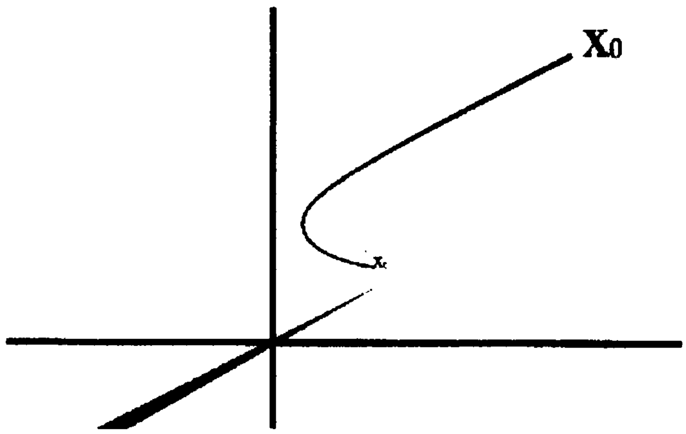


Figure 1.1: A phase space trajectory. The state of a system at $\mathbf{x}_0$, a point in phase space, and evolves over time, tracing a curve called a trajectory.

In all the following discussions the interest will be confined to dissipative systems. In this case, an initial volume in phase space will shrink as time evolves.

### 1.2.3 Lyapunov exponents

The relative flow on the attractor can be characterized by the Lyapunov exponents. These exponents measure how fast two infinitesimally close points in phase space will diverge on the average, as depicted in figure 1.2.

The Lyapunov exponent ($\lambda$) is then defined through the following equation

$$\lim_{r_0 \to 0} r_t = r_0 e^{\lambda t} \quad \text{for large } t \tag{1.3}$$

where $r$ is the distance between points in phase space. From (1.3) it is then

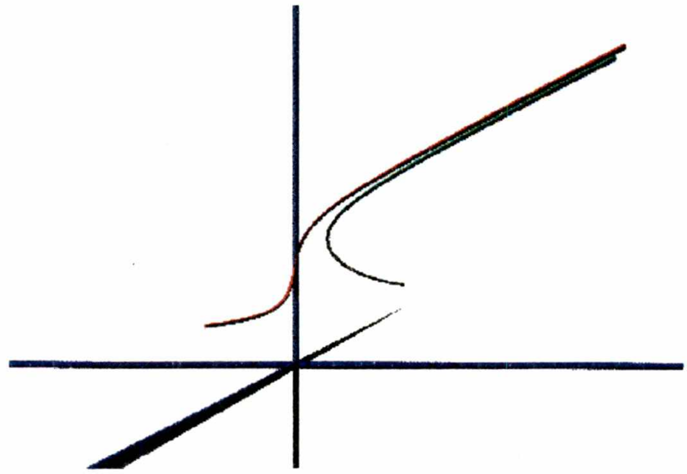

Figure 1.2: Sensitivity to initial conditions. Two systems that start out with almost identical initial conditions will diverge exponentially in a chaotic system.

easily seen that the trajectories will diverge exponentionally if $\lambda > 0$ and will converge exponentially if $\lambda < 0$ (the boundaries are $\lambda > 1$ and $\lambda < 1$ respectively, for discrete systems). Since the system lives in an $N$-dimensional space, $r$ can be oriented in $N$ independent directions. This means that there are $N$ Lyapunov exponents associated with an $N$-dimensional system. These are numbered $\{\lambda_i | i = 1, \dots, N\}$. Traditionally the exponents are ordered in descending magnitude. The largest exponent ($\lambda_1$) is associated with the largest diverging direction, the second largest exponent is associated with the largest diverging direction in the remaining space orthogonal to the first direction. Since the volume of an initial volume $V_0$ must decrease for dissipative systems, the sum of all Lyapunov exponents must be negative. Even in dissipative systems, however, the presence of even one positive Lyapunov exponent is sufficient to produce sensitivity to initial conditions.

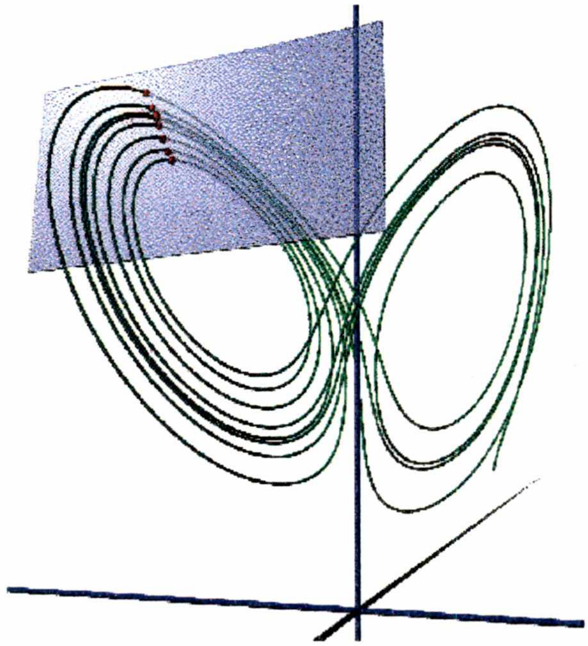

Figure 1.3: The Poincaré map. The sequence of intersections of the system trajectory with a plane forms the map.

### 1.2.4 Poincaré section

A tool that is often used in chaos analysis is the Poincaré section. This tool simplifies continuous systems by effectively turning them into discrete systems.

The method for obtaining a Poincaré section from a continuous system is by intersecting the trajectory of the system in phase space with a plane, as shown in figure 1.3. Each time the trajectory passes through the plane, a point is "mapped". The collection of mapped points is called the Poincaré section or Poincaré map.

A system exhibiting period one behavior records only one point on the

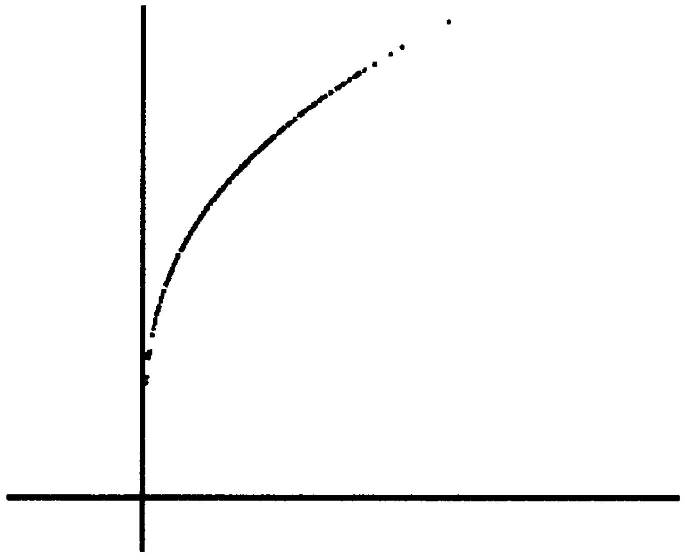

Figure 1.4: The Poincaré map of a chaotic system is a complex structure. The system never intersects at the same location.

Poincaré section, because it intersects the plane always at the same location. Similarly, a period two system draws two points on the section, et cetera. A chaotic system draws a highly structured and complex Poincaré section that never repeats itself (figure 1.4). In effect, a Poincaré section turns an $N$-dimensional continuous system into an $(N-1)$-dimensional discrete mapping of the plane onto itself.

### 1.2.5 Dynamics of a fixed point

Chaos control is based on exploitation of unstable periodic orbits that naturally occur in nonlinear systems. On the Poincaré map or in a regular discrete system, such orbits are represented by single or multiple discreet points. For simplicity, we consider here a single point map. In this case, the point of intersection is called a *fixed point* $\mathbf{x}_F$, and it is defined by

$$\mathbf{x}_F = \mathbf{F}(\mathbf{x}_F, \mathbf{p}, n) \tag{1.4}$$

It is important to note for future reference that $\mathbf{x}_F$ is a function of parameters $\mathbf{p}$.

The dynamics of fixed points can be classified in a number of different ways. One of the classification methods of interest concerns the stability of the fixed point after the trajectory is perturbed slightly away. This method discerns between the following classes:

- attractor: the system will tend to return to the fixed point (figure 1.5a).
- repeller: the system will tend to move further away from the fixed point (figure 1.5b).
- saddle: the fixed point is attracting in some directions (called the *stable manifold*) and repelling in others (called the *unstable manifold*). In effect, the system will approach the fixed point along the stable direction, and leave along the unstable direction, as shown in figure 1.5c.

In chaotic systems, many fixed points are naturally saddle points. This property is crucial for many control methods.

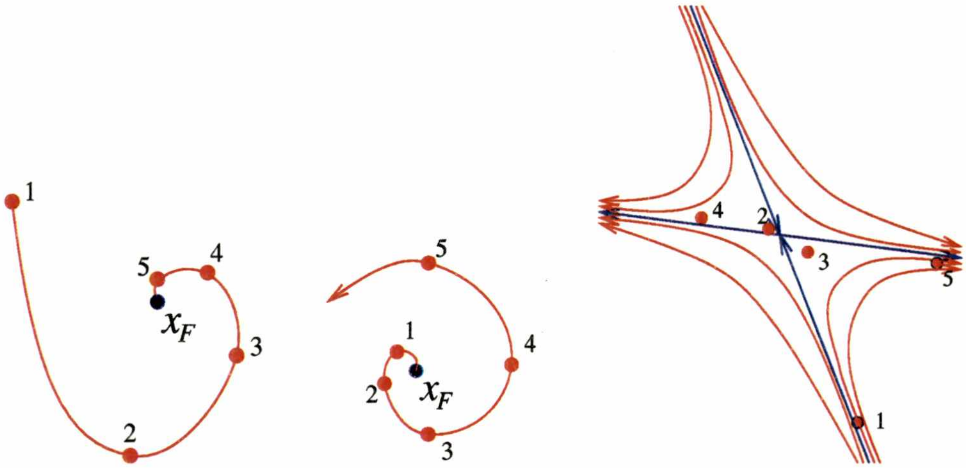


(a) attractor (b) repellor (c) saddle

Figure 1.5: Fixed points classification.

## 1.3 Chaos control

Ott, Grebogi, and Yorke created a breakthrough in the understanding of chaotic systems when they published a paper in 1990 outlining an algorithm which could eliminate chaos by making appropriately chosen feedback perturbations to a system parameter. Since this algorithm is the basis of many control strategies that followed, the fundamental concepts will be explained here.

### 1.3.1 OGY control

The basic principle underlying the OGY-method is the realization that a chaotic attractor is made up of an infinite number of unstable periodic orbits.

In a Poincaré section such orbits will produce an infinite collection of saddle points. The system "falls" from one unstable orbit onto another. In doing so, the system fills up the whole of the attractor, though some areas of the phase space are filled up more densely than others. This means that the system will come arbitrarily close to any desired location on the attractor at some point in the future.

The OGY-method waits for the system to land close to the desired fixed point. Once the system is close to the fixed point, the control algorithm perturbs a parameter $p$ such that the next iteration of the system falls onto the stable manifold of the unperturbed system. The system dynamics will then naturally draw the system state closer to the fixed point.

The geometrical and mathematical derivation of the algorithm is as follows. If the system comes close enough to the fixed point, it will land in the region around the fixed point where the linearization of the fixed point dynamics will be valid. These linear dynamics can then be expressed as follows:

$$\mathbf{x}_{n+1} - \mathbf{x}_F(p) = \mathbf{J}(\mathbf{x}_n - \mathbf{x}_F(p)) \tag{1.5}$$

where $\mathbf{J} \in \mathbb{R}^{N \times N}$ is the mapping matrix. For simplicity, we will assume $N = 2$ for the following discussion.

The dynamics of $\mathbf{M}$ are defined by its eigenvalues and eigenvectors:

$$\mathbf{J}\mathbf{v}_u = \lambda_u \mathbf{v}_u \tag{1.6}$$

$$\mathbf{J}\mathbf{v}_s = \lambda_s \mathbf{v}_s \tag{1.7}$$

where $\mathbf{v} \in \mathbb{R}^N$ are the eigenvectors and $\lambda \in \mathbb{R}$ are the eigenvalues (not to be mistaken for the Lyapunov exponents). The subscripts $u$ and $s$ refer to the *unstable* and *stable* directions respectively, in which the eigenvectors point. Since we are dealing with saddle points, the fixed point must have at least one stable and one unstable direction, shown in figure 1.5. In the following discussion, the eigenvectors are considered normalized ($\mathbf{v}^T\mathbf{v} = 1$).

Imagine now that the current state of the system is $\mathbf{x}_n$ as shown in figure 1.6a. The state of the system after the next iteration depends on the value of the nominal parameter $p_0$, and the perturbation $\Delta p$ we apply to it. To find an equation for $\mathbf{x}_{n+1}$, we have from (1.5)

$$\mathbf{x}_{n+1} = \mathbf{x}_F(p_0 + \Delta p) + \mathbf{J}(\mathbf{x}_n - \mathbf{x}_F(p_0 + \Delta p)) \tag{1.8}$$

expanding this into a first order Taylor series, we find

$$\mathbf{x}_{n+1} = \mathbf{x}_F(p) + \mathbf{s}\Delta p + \mathbf{J}(\mathbf{x}_n - \mathbf{x}_F(p) - \mathbf{s}\Delta p) \tag{1.9}$$

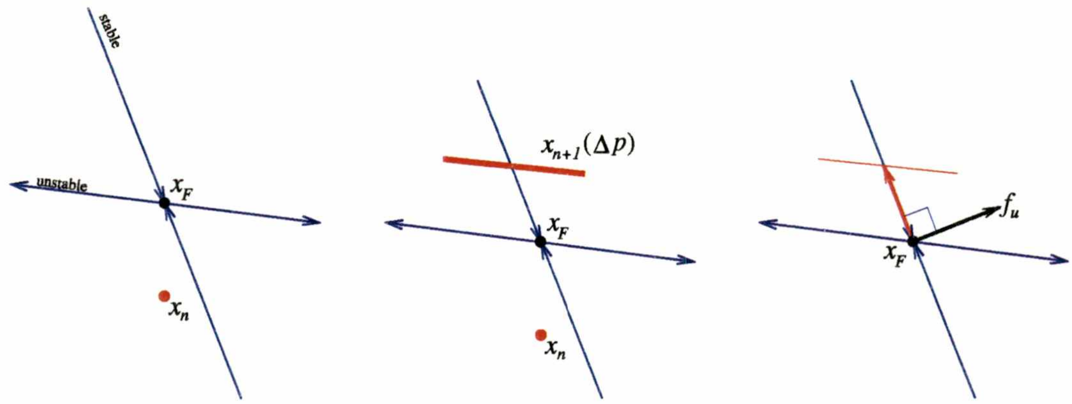


(a) The system lands close enough to the fixed point so that linearization is valid.

(b) The next system state $\mathbf{x}_{n+1}(\Delta p)$ depends linearly on $\Delta p$, and intersects with the stable manifold.

(c) To find the point on the stable manifold, we must find the vector on the $\mathbf{x}_{n+1}(\Delta p)$-line that is perpendicular to $\mathbf{f}_u$.

Figure 1.6: Steps in the OGY algorithm.

where

$$\mathbf{s} = \frac{\partial \mathbf{x}_F}{\partial p} \approx \frac{\mathbf{x}_F(p + \Delta p) - \mathbf{x}_F(p)}{\Delta p}$$

In (1.9) it is assumed that $\frac{\partial \mathbf{J}}{\partial p} \ll 1$. Equation (1.9) is a straight line and is shown in red in figure 1.6b. We can see from the figure that from the placement possibilities for $\mathbf{x}_{n+1}$, the one where (1.9) intersects with the stable manifold will be optimal when the desire is to draw the system closer to the fixed point.

The requirement that $\mathbf{x}_{n+1}$ be on the stable manifold can be expressed as the condition that $\mathbf{x}_{n+1} - \mathbf{x}_F(p)$ be perpendicular to a vector $\mathbf{f}_u$ that is perpendicular to the stable manifold[3](as shown in figure 1.6c), i.e., the inner product must be equal to zero:

$$\mathbf{f}_u^T(\mathbf{x}_{n+1} - \mathbf{x}_F(p)) = 0 \tag{1.10}$$

The vectors $\mathbf{f}_u$ and $\mathbf{f}_s$ (normal to the unstable manifold) are known as the *left eigenvectors* of $\mathbf{J}$, and are defined as

$$\begin{aligned} \mathbf{f}_u^T\mathbf{J} &= \lambda_u \mathbf{f}_u^T && (1.11) \\ \mathbf{f}_s^T\mathbf{J} &= \lambda_s \mathbf{f}_s^T && (1.12) \end{aligned}$$

The regular (right) and left eigenvectors are related through

$$\begin{bmatrix} \mathbf{f}_u \\ \mathbf{f}_s \end{bmatrix}^T = \begin{bmatrix} \mathbf{v}_u & \mathbf{v}_s \end{bmatrix}^{-1} \tag{1.13}$$

By combining (1.9) and (1.10) we find

$$0 = \mathbf{f}_u^T\mathbf{J}(\mathbf{x}_n - \mathbf{x}_F(p) - \mathbf{s}\Delta p) + \mathbf{f}_u^T\mathbf{s}\Delta p \tag{1.14}$$

Using (1.11) we then have

$$0 = \lambda_u\mathbf{f}_u^T(\mathbf{x}_n - \mathbf{x}_F(p) - \mathbf{s}\Delta p) + \mathbf{f}_u^T\mathbf{s}\Delta p \tag{1.15}$$

[3]this vector is also called a *normal* vector to a plane

Then substituting $\Delta \mathbf{x}_n = (\mathbf{x}_n - \mathbf{x}_F(p))$ and solving for $\Delta p$ we finally get the OGY formula:

$$\Delta p = \frac{\lambda_u}{\lambda_u - 1} \frac{\mathbf{f}_u^T \Delta \mathbf{x}_n}{\mathbf{f}_u^T \mathbf{s}} = \mathbf{c} \Delta \mathbf{x}_n \tag{1.16}$$

In essence, what this equations says is that the perturbation ($\Delta p$) needed for control is the inner product of the error ($\Delta \mathbf{x}_n$) and a vector ($\mathbf{c}$). This vector is a constant, and does not depend on the state of the system. The vector can be calculated once the Jacobian ($\mathbf{M}$) and the parameter Jacobian ($\mathbf{s}$) are determined from experimental data. Because of small errors due to linearization and small noise, equation (1.16) is not exact, and the parameter will have to be perturbed at every iteration, thus constantly driving the system back onto the stable manifold and closer to the fixed point.

Equation (1.16) places the system onto the stable manifold. This is not the only possible route to stabilizing the system. Romeiras, Grebogi, Ott, and Dayawansa (1992) derive a more general solution for every $\mathbf{c}$ that will theoretically stabilize the fixed point.

### 1.3.2 Comments on the OGY algorithm

#### Linear vs. nonlinear

Chaos happens only in nonlinear systems. The behavior of chaotic systems is highly complex, and for continuous systems, must move in at least three dimensions. Yet the derivation of (1.16), which achieves control, was done using purely linear methods. How is it that we can control a highly complex system like a chaotic system with a basically linear method? The answer is that the OGY algorithm implicitly uses the property of chaotic systems to explore the whole of their attractor. This property ensures that the system will naturally approach the desired fixed point, at which point the control method is activated. The control then does not have to use a great amount of power to shift the system to the desired state. Once the system is close enough, linearization becomes valid, and linear methods can be used to keep the system on the desired state. It will be seen later that dynamic noise can have the same exploring effect for nonlinear systems.

### Required system knowledge

It is noteworthy that equation (1.16) can in principle be determined without any prior knowledge or model of the system. Both $\mathbf{J}$ and $\mathbf{s}$ can be determined empirically from observed data. Even if not all state variables can be measured, there are *embedding* theorems that can transform a measured time series of any single system variable into a multi-dimensional attractor in phase space (Sauer, Yorke, and Casdagli 1991). The OGY control method was extended by Dressler and Nitsche (1992) to accommodate these "reconstructed" attractors. This, of course, sounds almost too good to be true: by measuring one variable over a period of time we can know everything about the system and can control it, expending virtually no energy. It has in fact been shown for models, as well as, controlled laboratory experiments that this does work.

In the real world, however, the situation is not so ideal. If one does not think in advance about the nature of the real system, there is a great risk that noise, spatial separation, etc., will decouple measurements from what really needs to be known, and measurements will be irrelevant. Careful prior consideration about what the dominating dynamics of the system will be, and what part of the dynamics are in fact of interest will be paramount for successful characterization and control. In the end, even an approximate system model is highly desirable.

### Multiple parameters

The original OGY control method only allows for one system parameter to be altered. For this reason, equation (1.9) has only one degree of freedom, as shown in figure 1.6b. To find an intersection with the stable manifold in general, the stable manifold must have dimension $N-1$. Imagine for example a three dimensional system where there is only one stable direction. In this case, both (1.9) and the stable manifold would be lines in a three dimensional space. The chance that they would intersect is infinitesimal. The system must have two stable directions in this case. It would appear that a system cannot have more than one unstable direction if it is to be controlled by the OGY method. Extrapolating: one needs as many independent perturbable parameters as one has unstable directions.[4] Derivation of a control law for multiple parameters follows.

First, (1.9) must be rewritten to accommodate multiple parameters:

$$\mathbf{x}_{n+1} - \mathbf{x}_F(\mathbf{p}) = \mathbf{S}\Delta\mathbf{p} + \mathbf{J}(\mathbf{x}_n - \mathbf{x}_F(\mathbf{p}) - \mathbf{S}\Delta\mathbf{p}) \tag{1.17}$$

where we now have an $N$-dimensional system with $N_u$ unstable directions and $N_s$ stable directions ($N = N_u + N_s$). In (1.17) we have $\Delta\mathbf{p} \in \mathbb{R}^{N_p = N_u}$ and $\mathbf{S} \in \mathbb{R}^{N \times N_u}$ is defined as

$$\mathbf{S} = \begin{bmatrix} | & & | \\ \frac{\partial \mathbf{x}_F}{\partial p_1} & \cdots & \frac{\partial \mathbf{x}_F}{\partial p_{N_u}} \\ | & & | \end{bmatrix}$$

We can easily rewrite (1.17) into

$$\Delta\mathbf{x}_{n+1} = \mathbf{J}\Delta\mathbf{x}_n + (\mathbf{S} - \mathbf{J}\mathbf{S})\,\Delta\mathbf{p} \tag{1.18}$$

Recall that we desire $\mathbf{x}_{n+1}$ to lie on the stable manifold, or, equivalently, $\Delta\mathbf{x}_{n+1}$ must lie in the plane spanned by the stable eigenvectors of $\mathbf{J}$. Then, any point on the stable manifold can be expressed as a linear combination of

[4]Chaotic systems with multiple unstable manifolds can in fact be controlled with only one parameter using a modified form of the original OGY method which uses a different criterion than (1.10), and that uses a pole placement technique, as described by Romeiras, Grebogi, Ott, and Dayawansa (1992)

the stable eigenvectors:

$$\mathbf{x} = \mathbf{V}_s \alpha \tag{1.19}$$

where $\mathbf{V}_s \in \mathbb{R}^{N \times N_s}$ and $\alpha \in \mathbb{R}^{N_s}$. To find the intersection we must then simply equate (1.18) and (1.19) to get

$$\mathbf{V}_s \alpha = \mathbf{J} \Delta \mathbf{x}_n + (\mathbf{S} - \mathbf{JS}) \, \Delta \mathbf{p} \tag{1.20}$$

which can be rearranged to

$$\mathbf{J} \Delta \mathbf{x}_n = \begin{bmatrix} (\mathbf{S} - \mathbf{JS}) & \mathbf{V}_s \end{bmatrix} \begin{bmatrix} \Delta \mathbf{p} \\ -\alpha \end{bmatrix} \tag{1.21}$$

Solving for $\Delta \mathbf{p}$ we obtain

$$\begin{bmatrix} \Delta \mathbf{p} \\ -\alpha \end{bmatrix} = - \begin{bmatrix} (\mathbf{S} - \mathbf{JS}) & \mathbf{V}_s \end{bmatrix}^{-1} \mathbf{J} \Delta \mathbf{x}_n \tag{1.22}$$

We are not interested in $\alpha$, so only the top $N_s$ elements of the left-hand side of (1.22) need to be calculated. Thus at every iteration, $\Delta \mathbf{x}_n$ needs to be multiplied with a fixed $N_s \times N$ matrix to obtain the needed parameter perturbations to drive the system onto the stable manifold.

A question to ask is whether getting the system on or close to the stable manifold is good enough to drive the system to the fixed point, would it not be better to in fact change the parameters so that the system is forced directly onto the fixed point, instead of onto the stable manifold. If the system is highly dissipative and if the noise level is low, the answer is most likely that putting the system close to the stable manifold will be good enough. However, if the system is only moderately dissipative, or very noisy, progress toward the fixed point may be slow, or ineffective.

It is interesting to consider an alternative approach which puts the next iterate directly onto the fixed point. To achieve this, we must expand the number of parameters used so that $N_p = N$. $\mathbf{x}_{n+1}$ can now be defined perfectly. The control law derivation is the same as above, except that $\mathbf{V}_s$ and $\alpha$ vanish, resulting in

$$\Delta\mathbf{p} = -\left(\mathbf{S} - \mathbf{JS}\right)^{-1}\mathbf{J}\Delta\mathbf{x}_n \tag{1.23}$$

Notice that there is no more need to find eigenvectors, only knowledge of $\mathbf{S}$ and $\mathbf{J}$ are required. The cost of this algorithm compared to regular OGY is of course that a greater amount of parameters must be accessible for perturbation.

## 1.4 Noise

### 1.4.1 Noise defined

An important question to consider is "what do we mean by *noise*?". Noise is present in any system, including the most accurate computer simulation. In the case of computers, an inherent source of noise is round-off error. Examples of noise in real systems include turbulent entrance and exit zones, external temperature and pressure changes, measurement errors, external vibration, and Brownian motion. For purposes of this discussion, noise is defined as

> high-dimensional dynamics — occurring either internal or external to our system — that perturb the system or our observations, but that are outside our direct scope of interest.

In effect, we consider noise as a secondary level of dynamics which does not totally dominate the behavior we are interested in, but does compromise our ability to observe the lower-dimensional features we care about.

### 1.4.2 Classifications

Noise can be classified as static (or measurement) noise or as dynamic noise (also called process disturbances). The first is due to our inability to measure the state of the system to infinite accuracy. Not only are our recording devices limited in their ability to store infinitely precise data, measurement devices add unknown dynamics (noise) to the signal. Thus the recorded signal is contaminated as follows:

$$\mathbf{y}_t = \mathbf{x}_t + \xi_t \tag{1.24}$$

where $\mathbf{y}_t$ is the measured system state, $\mathbf{x}_t$ is the actual system state, and $\xi_t$ is an unknown contamination of the signal. Since the contamination of the signal happens outside of the system, static noise does not directly influence the behavior of the system[5]. How to deal with this type of noise is discussed in many of the papers describing the many published algorithms that analyze chaotic data.

The second type of noise influences the behavior of the system directly. This dynamic noise is caused by unknown or unmodeled dynamics influencing the state variables. These dynamics can be internal, as well as, external to the system. A system being affected by dynamic noise can be written as

$$\dot{\mathbf{x}} = \mathbf{F}(\mathbf{x}, \mathbf{p}, \xi) \tag{1.25}$$

or

$$\mathbf{x}_{n+1} = \mathbf{F}(\mathbf{x}_n, \mathbf{p}, \xi_n) \tag{1.26}$$

Examples of dynamic noise are fluctuating input streams to chemical pro-

[5]Static noise could indirectly influence the system through a closed loop control system

cesses, changes in environment temperature and wave patterns running into ships at sea (Ding, Ott, and Grebogi 1994). The impact of dynamic noise on the behavior of a system can be quite dramatic. The sensitivity to perturbations described earlier can cause even a small amount of noise to totally change the behavior of the system.

Dynamic noise can be further subdivided into two different classes. With *additive noise*, we have

$$\dot{\mathbf{x}} = \mathbf{F}(\mathbf{x}, \mathbf{p}) + \xi_t \tag{1.27}$$

and

$$\mathbf{x}_{n+1} = \mathbf{F}(\mathbf{x}_n, \mathbf{p}) + \xi_n \tag{1.28}$$

In this case, the distribution function of the disturbance is independent of the system state, the noise is simply added to the system dynamics. For example, for the logistics system, we would have

$$x_{n+1} = \lambda x_n(1 - x_n) + \xi_n \tag{1.29}$$

The situation is more complicated with *multiplicative noise*

$$\dot{\mathbf{x}} = \mathbf{F}(\mathbf{x}, \mathbf{p} + \xi) \tag{1.30}$$

and

$$\mathbf{x}_{n+1} = \mathbf{F}(\mathbf{x}_n, \mathbf{p} + \xi_n) \tag{1.31}$$

Here, the noise distribution added to the dynamics becomes dependent on the state of the system. This is easily seen when written out for the logistics equations again

$$x_{n+1} = (\lambda + \xi_n)x_n(1 - x_n) = \lambda x_n(1 - x_n) + \xi_n x_n(1 - x_n) \tag{1.32}$$

Obviously, the second term in (1.32) is more complicated than the one in (1.29), even though the distribution of $\xi_n$ could be the same for both.

### 1.4.3 Literature review.

The area of dynamic noise in nonlinear and chaotic dynamics has remained relatively unexplored. Now that the fundamentals of chaotic dynamics have more or less matured, it appears more researchers are starting to explore how noise affects chaos. One of the earliest papers, by Mayer-Kress and Haken (1981), discusses the influence of noise on the Logistic Model. The authors added uniformly distributed noise to the model, as shown in equation (1.29). As the noise was added to periodic states of the model, Mayer-Kress and Haken observed two distinct behavior patterns. The first (shown in figure 1.7) causes a "reverse bifurcation" pattern as the noise level is increased. In

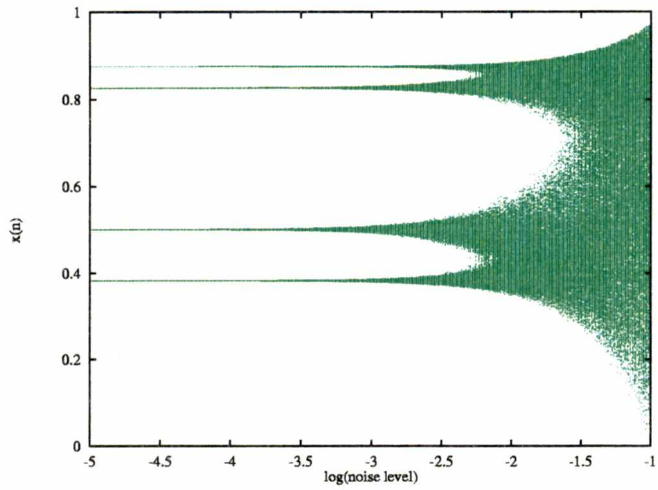


Figure 1.7: Reverse bifurcation: this pattern emerges when successively higher amounts of noise are added to certain system settings.

other words, points on the plane get smudged out and eventually merge with neighboring "smudges". These larger blobs continue on growing as noise is increased and merge with neighboring blobs, et cetera, until the whole picture is one large connected pattern.

The second type of behavior that Mayer-Kress and Haken observed was quite different, though they only changed the system parameter $\lambda$. In this case, the initial noise free points smudge out a little bit. But when the noise reaches a critical level, all of a sudden a completely new pattern emerges (shown in figure 1.8). This behavior is explained by unstable chaotic orbits being present. When the noise reaches a critical level, the system is knocked far away enough from the stable periodic orbit to be caught by the unstable chaotic orbits. The system will linger in the chaotic motion for a while and then return to the periodic motions, only to be knocked off again by the noise.

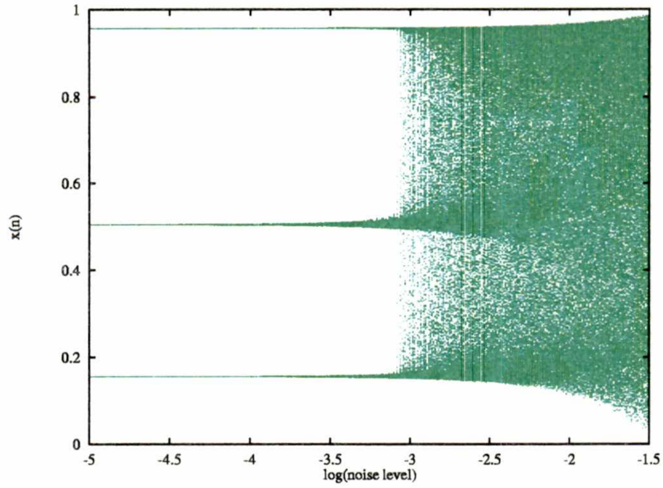


Figure 1.8: Attractor explosion: caused by noise knocking the system onto unstable chaotic orbits, the system "explodes".

Thus, once the threshold noise level has been reached, all of a sudden a much larger volume of the phase space gets explored. This behavior was further explored by Hamm, Tél, and Graham (1994), who discuss how this can lead to "noise-induced attractor explosion" and "noise-induced intermittency".

Christini and Collins (1995) in fact deliberately add noise to a periodic system to explore the phase space and to find unstable orbits that the periodic system would otherwise not visit. Once the system is near such a desired unstable orbit, OGY control is enabled and noise is switched off, thus locking the system into the unstable state.

Other authors, e.g., Matsumoto and Tsuda (1983), Wackerbauer (1995), Rajasekar (1995), and Fahy and Hamann (1992), have shown that dynamic noise can, in some cases, have a stabilizing effect on chaotic systems. Matsumoto and Tsuda attribute the *noise induced order* phenomenon in the

Belousov-Zhabotinsky reaction to "wide flat regions and narrow steep regions" in the B-Z map. The noise smears out the histogram, thus blurring the feedback process occurring in the system, which causes chaos. Herzel (1988) writes:

> ... the mechanism of Stabilization by Noise is quite general since most real noise sources should contain components which lead to the described "mixing of directions"

This means that because of the noise, directions in phase space will be mixed, which means that the dependence of the directions on the associated Lyapunov exponents will be smoothed. Since the total sum of the Lyapunov exponents must be negative, the eventual averaging of the directions and Lyapunov exponents will result in destroying chaos.

Another effect of noise, *stochastic resonance*, is discussed by Collins, Chow, and Imhoff (1995). This phenomenon allows the amplification of an input signal by a nonlinear system when a certain level of noise is present. Collins, Chow, and Imhoff show that this will even work for aperiodic inputs.

Thus, it is seen that dynamic noise can have a large variety of effects on nonlinear systems, and it is difficult to predict in advance what the effect will be. But some of these effects can be quite dramatic.

The area of control of nonlinear processes with noisy or irregular inputs remains virtually unexplored. Ding, Ott, and Grebogi (1994) show that OGY control can be used for systems with irregular inputs when the input can be predicted one cycle ahead of time. Christini and Collins (1995) use OGY control to lock on to a noisy unstable periodic orbit, but they deliberately add the noise to find this unstable orbit. Preliminary numerical experiments on the Hénon map have shown that the OGY control method is perhaps not the optimal control method for systems with a large amount of noise.

## 1.5 Research Plan

### 1.5.1 Conjectures to be tested

Control of chaotic processes that are influenced by large amounts of noise has so far not received wide attention. In real applications, however, this type of system is expected to be the rule rather than the exception. It has been shown that current chaos control algorithms do not perform optimally in the presence of large amounts of noise. The principle objective of the present research was to understand how the OGY control method might be adapted so as to improve the control of nonlinear systems exhibiting chaotic-like behavior under the influence of dynamic noise. The assumption will be made that the dynamic noise present cannot be eliminated or reduced, but must be dealt with through a control algorithm.

The basic approach taken involved making several conjectures regarding noisy chaotic behavior and the testing these conjectures in numerical experiments. The conjectures formulated were as follows:

**Conjecture 1** *The concepts of stable and unstable manifolds and fixed points can still be applied to nonlinear systems in the presence of dynamic noise.*

To study this conjecture, the following steps were taken

- Define the concepts of *fixed points* and *manifolds* in the context of noise.
- Demonstrate that these noisy structures converge to their classical counterparts in the limit as dynamic noise goes to zero.
- Develop practical procedures for estimating the noisy stable and unstable manifolds and fixed points.
- Evaluate how the fixed point and manifolds change with changing noise level.

**Conjecture 2** *The OGY control method can be adapted so as to accommodate and exploit the effects of dynamic noise on the system.*

To test this conjecture, the following steps were taken

- Define practically useful measures by which the success of feedback control in the presence of nonlinearly amplified noise can be quantified.
- Investigate how dynamic noise interferes with the control quality for traditional OGY control.

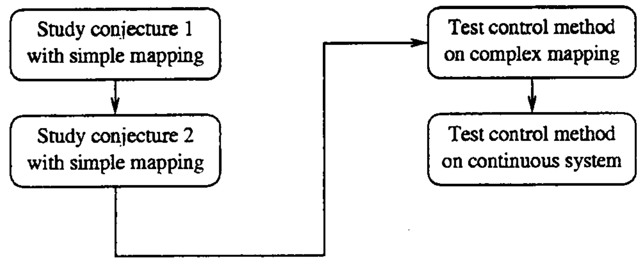


Figure 1.9: Outline of the steps to be taken for the proposed research.

- Adapt the OGY control method to be less sensitive to the effects of dynamic noise.

**Conjecture 3** *The developed control method is general enough to be applied to a variety of systems experiencing dynamic noise.*

To study this conjecture, methods developed above were tested on a variety of systems involving a range of complexity and relevance to engineering practice. Selected model systems will be discussed in the following section. The outline of the research is then shown in figure 1.9.

### 1.5.2 Selected model systems

#### Simple mapping

The general concepts were initially developed on two well known model systems. These models allowed demonstration of the developed methods in principle. To simplify simulation software, the model systems were mappings as opposed to a continuous system.

**The Hénon system** The first model system to be used in the development stage will be the Hénon map:

$$\begin{aligned} x_{n+1} &= 1 - a x_n^2 + y_n \\ y_{n+1} &= b x_n \end{aligned} \tag{1.33}$$

This two dimensional model is very simple, and has been widely studied. It is now one of the most often used paradigms in chaos theory. This model has already been used for the preliminary studies discussed above, and simulation software for it already exists. One drawback of the Hénon system is that it tends to become unstable when noise is added when the system is nominally in a chaotic mode. The noise causes the system to be knocked out of the chaotic attraction basin, and the system state rapidly grows to infinity. Another concern is that the Hénon map might be considered "too ideal", i.e., algorithms that have been shown to work well for this system have failed to work on more complex systems.

**The Ikeda system** A more complex, but still widely studied, model is the Ikeda map (Ikeda 1979). The model describes the behavior of a ring cavity optical system.

$$z_{n+1} = p + Bz_n \exp\left[ik - i\frac{\alpha}{1 + |z_n|^2}\right] \tag{1.34}$$

where $z = x + iy$ is a complex number. This system does not suffer from "blow-up" like the Hénon map does. It is, however, much more sensitive to noise in the sense that less amounts of noise are required to make the system very complex.

### Application of the method to a realistic discrete model

The initial test of generality and usefulness of the developed method will be to apply it to a more complex and more realistic model. The system used for this purpose is a model of an internal combustion engine (Daw, Finney, Green, Kennel, Thomas, and Connolly 1996). The model is a cycle to cycle mapping of the form

$$\begin{bmatrix} m_{i+1} \\ a_{i+1} \end{bmatrix} = \mathbf{F}(\begin{bmatrix} m_i \\ a_i \end{bmatrix}) \tag{1.35}$$

where $m_i$ is the fuel mass in the cylinder at cycle $i$, and $a_i$ the air mass. As a convention the system is reported in terms of the *heat release* per cycle:

$$hr_i = g(m_i, a_i) \tag{1.36}$$

For chaos purposes return maps of $hr_i$ are plotted, usually in two dimensions. Such a plot is shown in figure 3.12a.

### Application of the method to a realistic continuous model

The second model test examined how well the method works for continuous systems. With continuous systems, there is the problem that the noise will also be continuous and could thus have a very different impact on the dynamics of the system. An added questions is "what would be an appropriate way to add noise to a continuous model?".

Jorgensen and Aris (1983) developed a model for a simple consecutive chemical reaction system ($A \rightarrow B \rightarrow C$) in a stirred tank reactor. The model was derived by simple mass and energy balances:

$$
\begin{aligned}
V\frac{\partial c_A}{\partial t'} =& q(c_{Af} - c_A) - V c_A A_1 \exp(-\frac{E_1}{RT}) \\
V\frac{\partial c_B}{\partial t'} =& q(c_{Bf} - c_B) + V c_A A_1 \exp(-\frac{E_1}{RT}) - V c_B A_2 \exp(-\frac{E_2}{RT}) \\
V\rho c_p \frac{\partial T}{\partial t'} =& q\rho c_p(T_f - T) + (-\Delta H_1) V c_A A_1 \exp(-\frac{E_1}{RT}) + \\
& (-\Delta H_2) V c_B A_2 \exp(-\frac{E_2}{RT}) - UA_c(T - T_c)
\end{aligned}
$$

The meaning of the symbols is listed in the Appendix. Using the dimensionless variables and numbers listed in the Appendix, the equations can be written in dimensionless form

$$\begin{aligned}
\frac{\partial u}{\partial t} &= 1 - u(1 + \alpha e^{w}) \\
\frac{\partial v}{\partial t} &= \alpha u e^{w} - v(1 + \alpha \sigma e^{w}) \\
\frac{\partial w}{\partial t} &= -(1 + \kappa) w + \alpha \beta u e^{w} + \alpha \beta h \sigma v e^{w}
\end{aligned} \tag{1.37}$$

Integrating system (1.37) is in itself an interesting exercise in the study of the effects of dynamics noise on nonlinear systems. The equations are stiff due to a sharp temperature peak in the solution. As a result, this system is very sensitive to numerical noise caused by round-off errors in the integration algorithm. Figure 1.10 shows a number of solutions to the system using the same system settings, but different error tolerances in the integration algorithm. Notice that the solutions vary significantly, depending on the numerical noise level. Additionally, different integration algorithms give different solutions. Algorithms tried included Rosenbrock methods (Shampine, as well as, Kaps and Rentrop parameter sets), Semi-implicit extrapolation methods (both methods described by Press, Teukolsky, Vetterling, and Flannery (1992)), and routines supplied by Matlab 5.1. None of the methods could match the solutions found by Jorgensen and Aris (1983). Prohibitive computation times did not allow for more exact solutions, so that it is difficult to say whether the "true" solution will be chaotic or not. In any case, it is not really relevant, since in an engineering environment there are no exact solutions, and the engineer will always have to deal with the system as it is

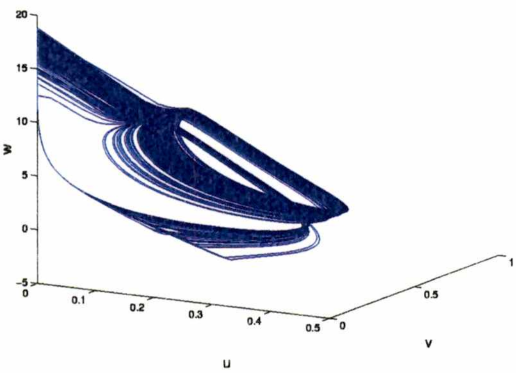


(a) Relative error tolerance = $1 * 10^{-2}$

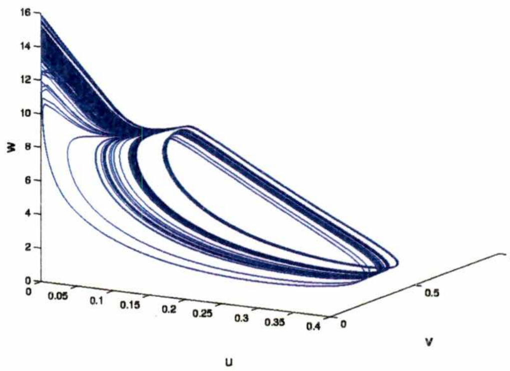


(b) Relative error tolerance = $1 * 10^{-4}$

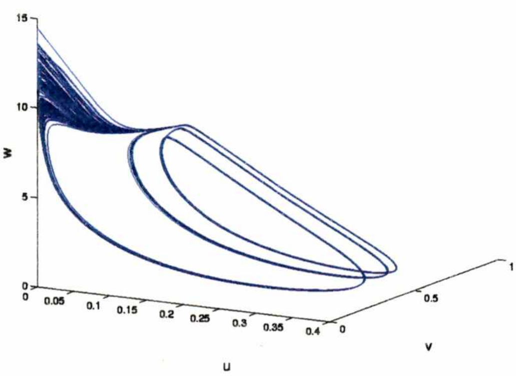


(c) Relative error tolerance = $1 * 10^{-6}$

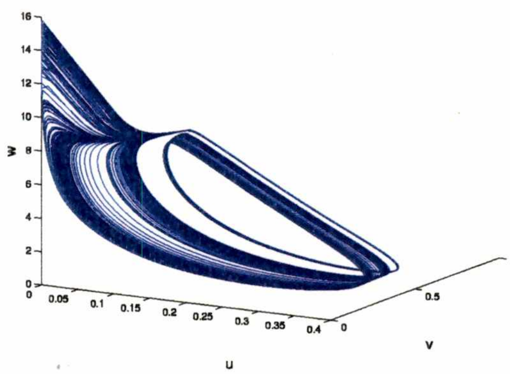


(d) Relative error tolerance = $1 * 10^{-8}$

Figure 1.10: Chaotic solutions of the CSTR model. Parameter values are: $\alpha = 0.55$, $\beta = 17.5$, $h = 1.0$, $\sigma = 0.01$, and $\kappa = 7.286670$. The different solutions were obtained by varying the error tolerance in the integration algorithm.

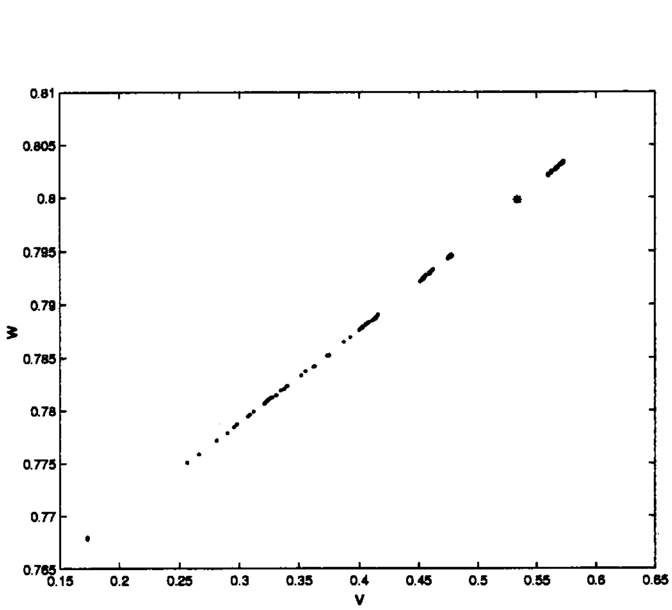


Figure 1.11: Poincaré section of the CSTR model. The section plane is $u = 0.2192$. The fixed point has been indicated with a red $*$.

influenced by noise. In all subsequent calculation the relative error tolerance was set to $10^{-8}$. The integration algorithm used was Matlab routine `ode15s`, which is a variable order method.

Since the developed methods act on mapped systems, it is necessary to take a Poincaré section of the solution. The section used was taken through the plane $u = 0.2192$. A plot of this mapping is shown in figure 1.11.

To add realistic disturbances to the system, Gaussian noise was added to the feed concentration $c_{Af}$. The frequency of the noise was determined by taking the peak frequency in the power spectrum (figure 1.12). Note how sharp the peaks in the spectrum are. This indicates that the system is only barely chaotic. In fact, the fixed point of the system is only slightly unstable with an unstable eigenvalue of $-1.06$. The corresponding stable eigenvalue

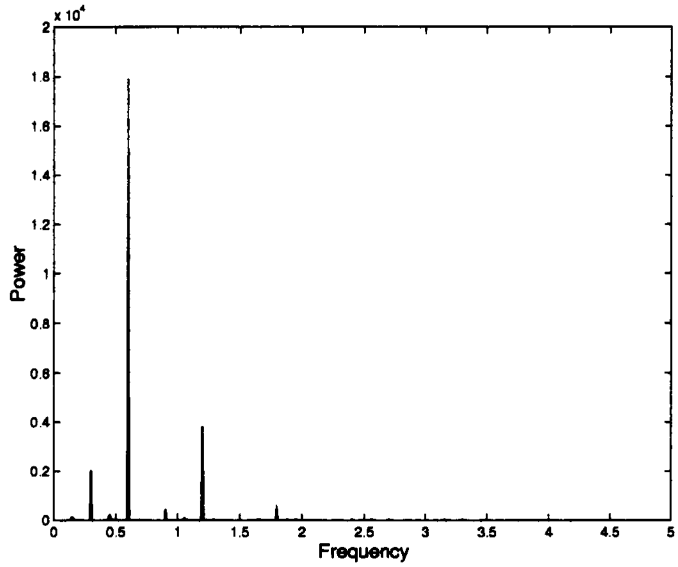


Figure 1.12: Power spectrum of the CSTR model.

is $-0.384$. The highest peak in the power spectrum is located at a frequency of 0.6. The dimensionless time in the system is relative to the residence time in the reactor. The dominant time scale in the reactor is then about 1.66 residence times. The noise added to the feed concentration was changed at that particular frequency.

The effect of different noise levels is shown in figure 1.13. Notice the similarities between the effects of added noise levels and numerical noise levels (figure 1.10). For the numerical control experiments, a noise level of $10^{-2}$ was chosen. The Poincar'e map for this setting is shown in figure 1.14.

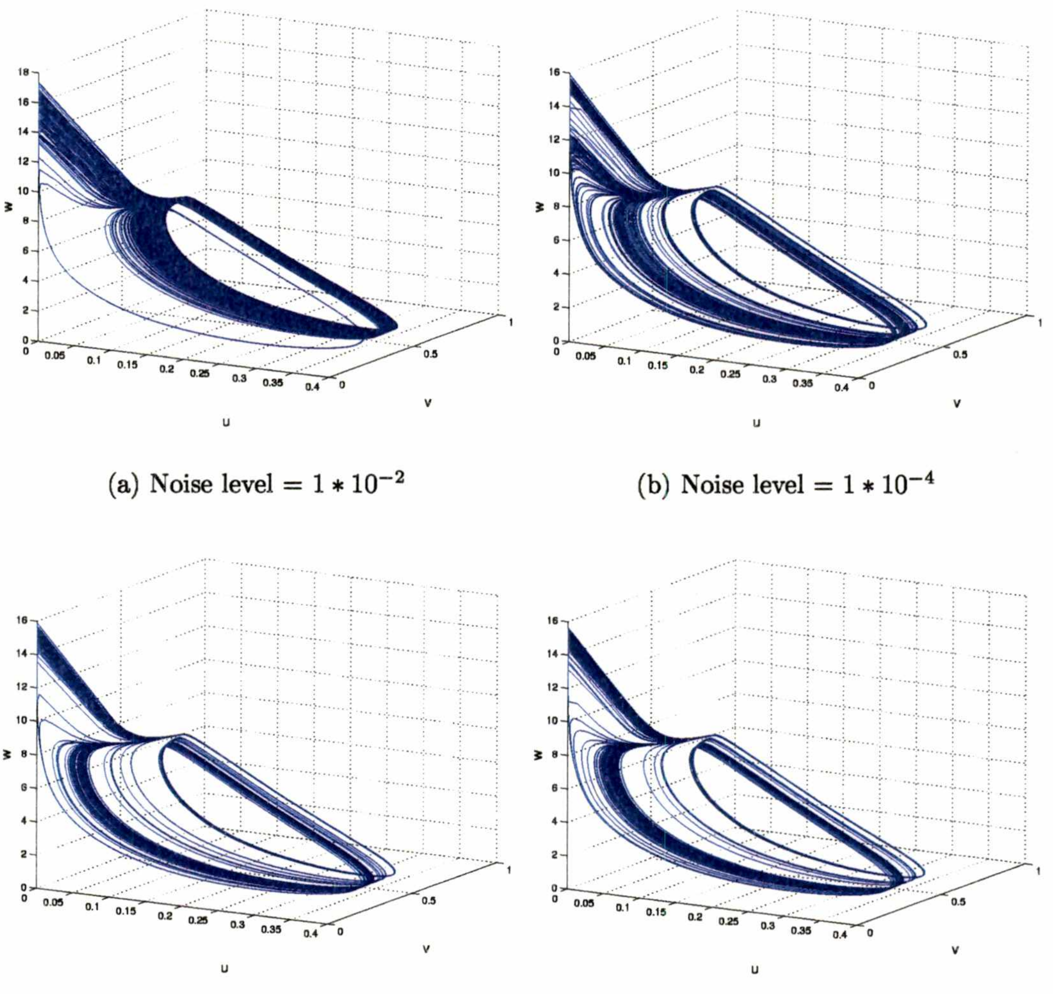


(a) Noise level = $1 * 10^{-2}$

(b) Noise level = $1 * 10^{-4}$

(c) Noise level = $1 * 10^{-6}$

(d) Noise level = $1 * 10^{-8}$

Figure 1.13: Chaotic solutions of the CSTR model with added dynamic noise. Noise was added to the $\beta$ parameter.

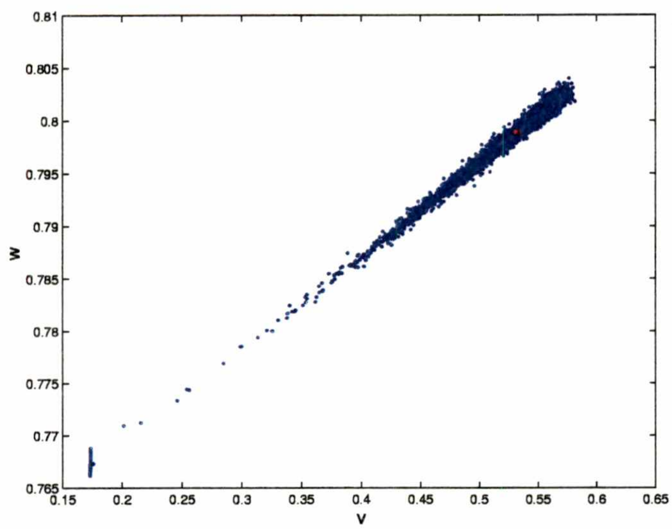


Figure 1.14: Poincare map of the noisy CSTR system.

# Chapter 2

# Dynamic structure concepts

## 2.1 Fixed point definition

In the field of nonlinear dynamics, a great deal revolves around the concept of *fixed points.* In classical systems (without noise), these fixed points are defined as

$$\mathbf{x}_F = \mathbf{F}(\mathbf{x}_F) \tag{2.1}$$

This means that with initial condition $\mathbf{x}_F$, the state of the system will never change. When dynamic noise is added to the system, however, this definition is no longer strictly valid. Since the system constantly changes with the addition of noise, the system will virtually never remain static, as it is in equation (2.1). Another definition is then needed for the concept of a fixed

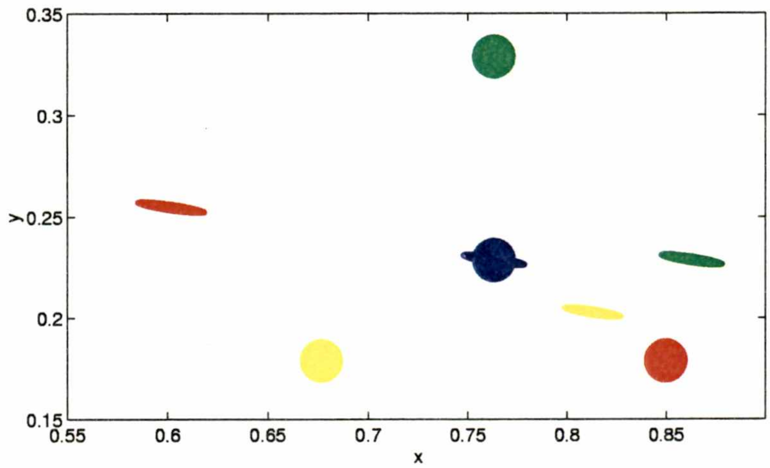


Figure 2.1: Circles of radius 0.01 are transformed into ellipses after one iteration of the Hénon map without noise. The different colors correspond to "before" and "after". The blue areas correspond to the actual fixed point.

point in the context of noise.

A definition, which becomes apparent from figure 2.1, can be stated as follows:

**Definition 2.1** *Given a small spherical volume of initial points, centered at* $\mathbf{x}_{Fn}$*, the fixed point in the context of noise is defined as that* $\mathbf{x}_{Fn}$ *at which the Euclidean distance* $r_{Fn}$ *between* $\mathbf{x}_{Fn}$*, and the mean of the spheroid after one iteration, is minimized.*

In the no noise case, $r_{Fn}$ should approach zero. This definition was initially tested using the Hénon map with parameter values $[a, b] = [0.8, 0.3]$. For the no noise case, a surface plot of the neighborhood of the fixed point was constructed to observe the local structure. This plot is shown in figure 2.2. The surface appears nice and smooth, with the minimum at the desired fixed

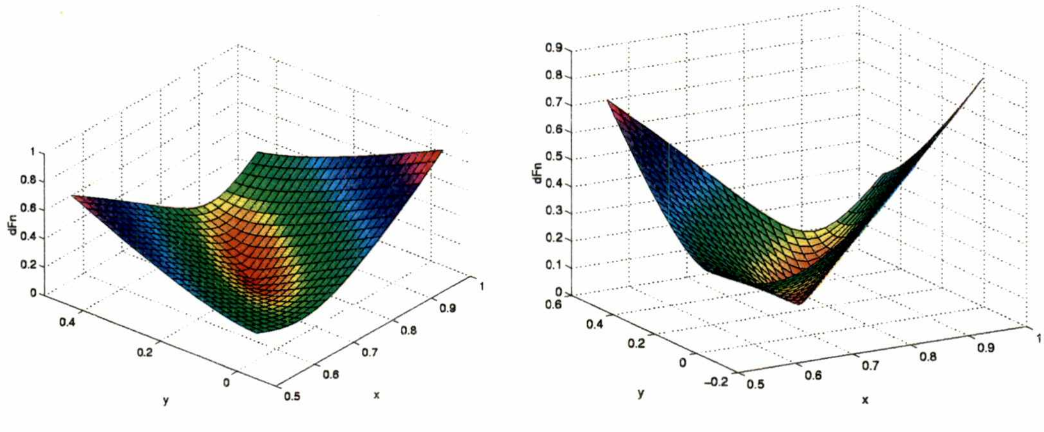


Figure 2.2: Surface of $d_{Fn}$ in the neighborhood of the fixed point for the Hénon map. The two plots show different view angles of the same surface.

point. The minimum was found by using the simplex algorithm, as described by Press, Teukolsky, Vetterling, and Flannery (1992).

## 2.2 Fixed point drifting under the influence of Gaussian noise

### 2.2.1 Hénon map

To observe how the fixed point is affected by different levels of Gaussian noise, the fixed point was determined for the Hénon map at different levels of noise and with three different parameter values. Gaussian noise was chosen because it is expected to be the most common type observed in experimental systems. The fixed point was located using definition 2.1. The results are shown in table 2.1. The noise level is defined in terms of the standard deviation of the perturbation to $a$. On each iterate the actual $a$ used is given by $a = \hat{a} + \epsilon$, where $\hat{a}$ is the nominal (mean) value and $\epsilon$ is Gaussian distributed with mean zero.

From the table, it can be seen that noise on one parameter does not appear to shift the position of the fixed point. A similar experiment was done by adding noise to both parameters in the Hénon map. These results are shown in table 2.2. From this experiment it also appears that the location of the fixed point as defined does not shift under the influence of noise.

### 2.2.2 The Ikeda map

To test whether the nonshifting of the fixed point under the influence of noise is particular to the Hénon map, a similar experiment was performed for the Ikeda map, equation (1.34). The results are shown in table 2.3. Again, Gaussian noise does not appear to influence the location of the fixed point.

## 2.3 Manifold definition

As with the fixed point, the theoretical definitions of stable and unstable manifolds do not really hold when the system is very noisy. New definitions, in the context of noise, are then required.

The manifolds in the linear neighborhood of the fixed point are defined along the eigenvectors of the Jacobian of the system at the fixed point. Eigen-

Table 2.1: The fixed point for the Hénon map is determined for different parameters as well as different noise levels on the $a$ parameter. The noise is Gaussian. At $\hat{a} = 0.25$, the map is in a period one state, for $\hat{a} = 0.8$, the map is in period two, and for $\hat{a} = 1.15$ the motion is chaotic ($b = 0.3$ for all runs). The estimation was done using 100000 random data points and an error tolerance of $5 * 10^{-5}$.

| | $\hat{a} = 0.25$ | | $\hat{a} = 0.8$ | | $\hat{a} = 1.15$ | |
|---|---|---|---|---|---|---|
| Noise level | $x$ | $y$ | $x$ | $y$ | $x$ | $y$ |
| 0.00 | 1.0413 | 0.3124 | 0.7631 | 0.2289 | 0.6766 | 0.2030 |
| $1.00 * 10^{-6}$ | 1.0413 | 0.3124 | 0.7631 | 0.2290 | 0.6766 | 0.2030 |
| $2.00 * 10^{-6}$ | 1.0413 | 0.3124 | 0.7631 | 0.2290 | 0.6765 | 0.2029 |
| $4.00 * 10^{-6}$ | 1.0413 | 0.3124 | 0.7631 | 0.2289 | 0.6766 | 0.2030 |
| $8.00 * 10^{-6}$ | 1.0413 | 0.3123 | 0.7631 | 0.2289 | 0.6765 | 0.2029 |
| $1.60 * 10^{-5}$ | 1.0413 | 0.3123 | 0.7631 | 0.2289 | 0.6766 | 0.2030 |
| $3.20 * 10^{-5}$ | 1.0413 | 0.3124 | 0.7631 | 0.2289 | 0.6766 | 0.2030 |
| $6.40 * 10^{-5}$ | 1.0413 | 0.3123 | 0.7631 | 0.2289 | 0.6766 | 0.2030 |
| $1.28 * 10^{-4}$ | 1.0413 | 0.3124 | 0.7631 | 0.2290 | 0.6766 | 0.2030 |
| $2.56 * 10^{-4}$ | 1.0413 | 0.3124 | 0.7630 | 0.2290 | 0.6766 | 0.2030 |
| $5.12 * 10^{-4}$ | 1.0413 | 0.3124 | 0.7631 | 0.2289 | 0.6766 | 0.2030 |
| $1.02 * 10^{-3}$ | 1.0413 | 0.3123 | 0.7631 | 0.2289 | 0.6765 | 0.2029 |
| $2.04 * 10^{-3}$ | 1.0412 | 0.3123 | 0.7631 | 0.2289 | 0.6766 | 0.2030 |
| $4.10 * 10^{-3}$ | 1.0413 | 0.3123 | 0.7630 | 0.2290 | 0.6766 | 0.2030 |
| $8.19 * 10^{-3}$ | 1.0413 | 0.3125 | 0.7631 | 0.2290 | 0.6765 | 0.2029 |
| $1.64 * 10^{-2}$ | 1.0413 | 0.3124 | 0.7631 | 0.2289 | 0.6765 | 0.2029 |
| $3.28 * 10^{-2}$ | 1.0414 | 0.3125 | 0.7631 | 0.2289 | 0.6765 | 0.2030 |
| $6.55 * 10^{-2}$ | 1.0415 | 0.3125 | 0.7631 | 0.2289 | 0.6765 | 0.2029 |

Table 2.2: The fixed point for the Hénon map is determined for different parameters as well as different noise levels on the $a$ as well as the $b$ parameter. The noise is Gaussian. At $\hat{a} = 0.25$, the map is in a period one state, for $\hat{a} = 0.8$, the map is in period two, and for $\hat{a} = 1.15$ the motion is chaotic ($\hat{b} = 0.3$ for all runs). The estimation was done using 100000 random data points and an error tolerance of $5 * 10^{-5}$.

| | $\hat{a} = 0.25$ | | $\hat{a} = 0.8$ | | $\hat{a} = 1.15$ | |
|---|---|---|---|---|---|---|
| Noise level | $x$ | $y$ | $x$ | $y$ | $x$ | $y$ |
| 0.00 | 1.0413 | 0.3124 | 0.7631 | 0.2289 | 0.6766 | 0.2030 |
| $1.00 * 10^{-6}$ | 1.0413 | 0.3124 | 0.7631 | 0.2289 | 0.6766 | 0.2030 |
| $4.00 * 10^{-6}$ | 1.0413 | 0.3124 | 0.7631 | 0.2289 | 0.6765 | 0.2030 |
| $1.60 * 10^{-5}$ | 1.0413 | 0.3124 | 0.7630 | 0.2290 | 0.6766 | 0.2030 |
| $6.40 * 10^{-5}$ | 1.0413 | 0.3124 | 0.7631 | 0.2290 | 0.6765 | 0.2029 |
| $2.56 * 10^{-4}$ | 1.0413 | 0.3124 | 0.7631 | 0.2290 | 0.6766 | 0.2030 |
| $1.02 * 10^{-3}$ | 1.0413 | 0.3124 | 0.7631 | 0.2289 | 0.6765 | 0.2029 |
| $4.10 * 10^{-3}$ | 1.0413 | 0.3124 | 0.7631 | 0.2290 | 0.6765 | 0.2030 |
| $1.64 * 10^{-2}$ | 1.0412 | 0.3122 | 0.7630 | 0.2289 | 0.6765 | 0.2029 |
| $6.55 * 10^{-2}$ | 1.0413 | 0.3123 | 0.7634 | 0.2291 | 0.6765 | 0.2029 |

values and eigenvectors are defined through the equation

$$\mathbf{M}\mathbf{v} = \lambda\mathbf{v} \tag{2.2}$$

where $\mathbf{M}$ is a square matrix $M \in \mathbb{R}^{d \times d}$, $\mathbf{v} \in \mathbb{R}^d$ is an eigenvector, and $\lambda \in \mathbb{C}$ is the corresponding eigenvalue for any non-trivial solution of 2.2. From the equation, it is seen that any vector that is a multiple of the eigenvector $\mathbf{x}$ merely gets scaled by a factor $\lambda$ when multiplied by $\mathbf{M}$. That is, any vector along $\mathbf{x}$ does not change direction. This observation naturally leads to the following definition of manifolds in the context of noise.

**Definition 2.2** *Define a small wedge* $\mathbf{A}$ *(with angle* $\alpha$*) from a small circle*

Table 2.3: The fixed point for the Ikeda map is determined for different parameters as well as different noise levels on the $B$ parameter. The noise is Gaussian. At $\hat{B} = 0.3$, the map is in a period one state, for $\hat{B} = 0.55$, the map is in period two, and for $\hat{B} = 0.76$ the motion is chaotic ($\alpha = 6.0$, $p = 1.0$, and $K = 0.4$ for all runs). The estimation was done using 200000 random data points and an error tolerance of $5 * 10^{-5}$.

| | $\hat{B} = 0.30$ | | $\hat{B} = 0.55$ | | $\hat{B} = 0.76$ | |
|---|---|---|---|---|---|---|
| Noise level | $x$ | $y$ | $x$ | $y$ | $x$ | $y$ |
| 0.00 | 0.7715 | 0.03838 | 0.6575 | 0.1385 | 0.5803 | 0.2084 |
| $1.00 * 10^{-6}$ | 0.7715 | 0.03838 | 0.6575 | 0.1385 | 0.5803 | 0.2084 |
| $2.00 * 10^{-6}$ | 0.7715 | 0.03838 | 0.6575 | 0.1385 | 0.5803 | 0.2084 |
| $4.00 * 10^{-6}$ | 0.7715 | 0.03838 | 0.6575 | 0.1385 | 0.5803 | 0.2084 |
| $8.00 * 10^{-6}$ | 0.7715 | 0.03838 | 0.6575 | 0.1385 | 0.5803 | 0.2083 |
| $1.60 * 10^{-5}$ | 0.7715 | 0.03838 | 0.6575 | 0.1385 | 0.5804 | 0.2083 |
| $3.20 * 10^{-5}$ | 0.7715 | 0.03838 | 0.6575 | 0.1385 | 0.5803 | 0.2084 |
| $6.40 * 10^{-5}$ | 0.7715 | 0.03838 | 0.6575 | 0.1385 | 0.5804 | 0.2083 |
| $1.28 * 10^{-4}$ | 0.7715 | 0.03838 | 0.6575 | 0.1385 | 0.5803 | 0.2083 |
| $2.56 * 10^{-4}$ | 0.7715 | 0.03838 | 0.6575 | 0.1385 | 0.5803 | 0.2083 |
| $5.12 * 10^{-4}$ | 0.7715 | 0.03838 | 0.6575 | 0.1385 | 0.5804 | 0.2083 |
| $1.02 * 10^{-3}$ | 0.7715 | 0.03838 | 0.6575 | 0.1385 | 0.5803 | 0.2083 |
| $2.04 * 10^{-3}$ | 0.7715 | 0.03837 | 0.6575 | 0.1385 | 0.5803 | 0.2084 |
| $4.10 * 10^{-3}$ | 0.7715 | 0.03838 | 0.6575 | 0.1385 | 0.5803 | 0.2083 |
| $8.19 * 10^{-3}$ | 0.7715 | 0.03837 | 0.6575 | 0.1385 | 0.5803 | 0.2084 |
| $1.64 * 10^{-2}$ | 0.7715 | 0.03837 | 0.6575 | 0.1385 | 0.5803 | 0.2083 |
| $3.28 * 10^{-2}$ | 0.7715 | 0.03840 | 0.6575 | 0.1385 | 0.5803 | 0.2084 |
| $6.55 * 10^{-2}$ | 0.7715 | 0.03835 | 0.6575 | 0.1385 | 0.5803 | 0.2084 |

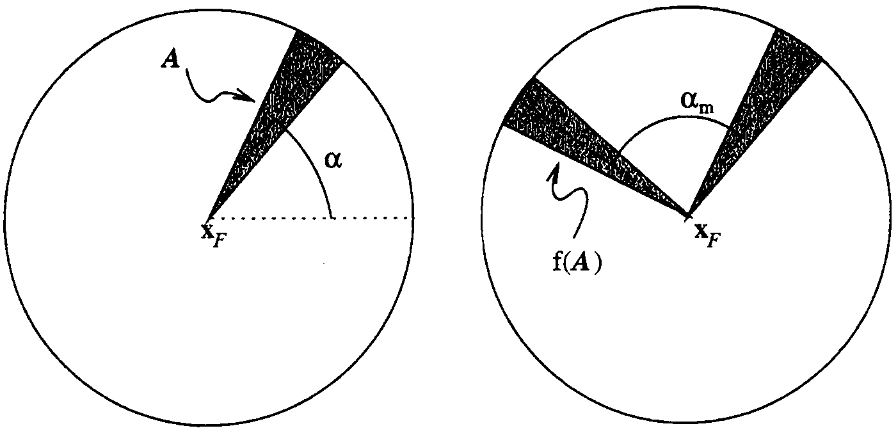


(a) (b)

Figure 2.3: Determination of the manifold structure. **A** is along an eigenvector when $\alpha_m$ is minimized.

*centered at the fixed point* $\mathbf{x}_F$ *(see figure 2.3a). Define* $\alpha_m$ *as the angle between* **A** *and the once iterated map of* **A**, *as shown in figure 2.3b. The manifolds are then defined where* $\alpha_m$ *is minimized.*

The definition was tried out on the noise free Hénon map to verify that the definition does indeed give the manifolds for the noise free case. A graph of the results — shown in figure 2.4 — clearly touches $\alpha_m = 0$ in two places within half a circle's circumference. These points in the graph correspond to the theoretical manifold angles, which are 0.96 for the stable manifold and 2.93 for the unstable manifold.

A corresponding definition for eigenvalues in the context of noise is then easily stated:

**Definition 2.3** *Given a small wedge* **A** *lying on a manifold as defined by*

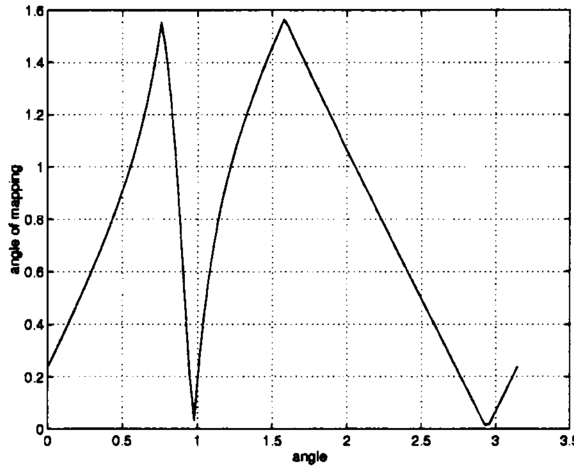


Figure 2.4: Manifolds for the noise free Hénon map.

*definition 2.2, define* $\mathbf{w}_0 \in \mathbb{R}^d$ *as the average vector in* $\mathbf{A}$. *Also define* $\mathbf{w}_1 \in \mathbb{R}^d$ *as the average vector in the once iterated map of* $\mathbf{A}$. *The corresponding eigenvalue in the context of noise is then defined as*

$$\lambda = \operatorname{sgn}(||\mathbf{w}_0 + \mathbf{w}_1|| - ||\mathbf{w}_0 - \mathbf{w}_1||)\frac{||\mathbf{w}_1||}{||\mathbf{w}_0||}$$

Note that the sgn() term identifies whether the eigenvalue is positive or negative.

## 2.4 Manifold shifting under the influence of Gaussian noise

Since dynamic noise influences the dynamics of the system, it is reasonable to suspect that noise causes the manifold structure of fixed points to be altered.

To investigate this effect, the manifold and eigenvalue shifting was examined for the Hénon map.

To observe shifting, the manifold and eigenvalues for the Hénon map fixed point were determined for different levels of noise present in the system as well as for different nominal parameter settings. The chosen parameters are the same as described in the previous experiment, i.e., $a = 0.25$ gives a nominally period one solution, $a = 0.80$ is a period two, and $a = 1.15$ is a chaotic solution. The results are shown in figure 2.5.

The figures clearly show that the manifolds and eigenvalues do shift as more and more noise is added to the system. The manifold angles asymptotically approach $\frac{\pi}{2}$ as the noise level increases. At $\sigma = \infty$, noise completely controls the system, and the distribution of the manifold angles will be uniform over $[0, \pi]$, the mean of which will be $\frac{\pi}{2}$. Equivalently, the eigenvalues asymptotically approach $\pm 1$. Eigenvalues of $\pm 1$ signify that there is no expansion or contraction of the system in that particular direction, which is what one would expect on the average when the system is dominated by noise.

Similar results are obtained for the Ikeda map, as illustrated in figure 2.6.

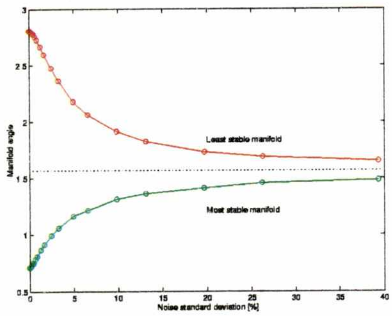


(a) Manifolds for $\hat{a} = 0.25$ and $b = 0.3$.

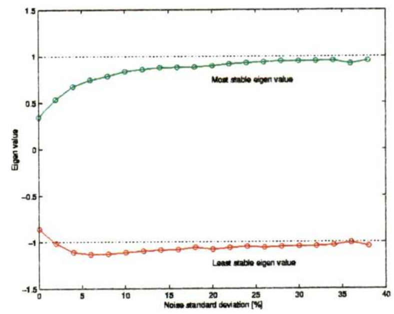


(b) Eigenvalues for $\hat{a} = 0.25$ and $b = 0.3$.

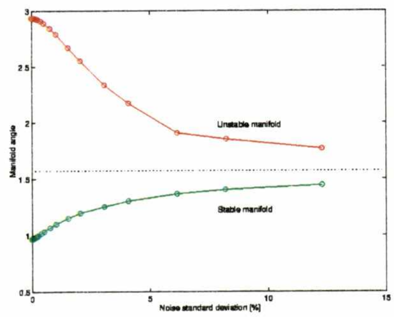


(c) Manifolds for $\hat{a} = 0.80$ and $b = 0.3$.

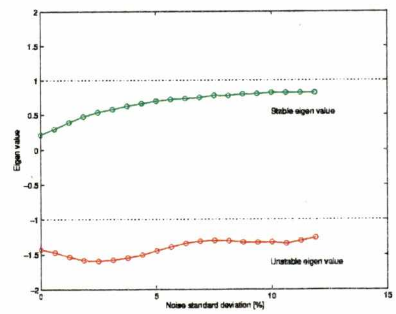


(d) Eigenvalues for $\hat{a} = 0.80$ and $b = 0.3$.

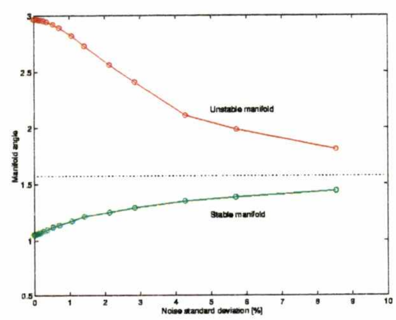


(e) Manifolds for $\hat{a} = 1.15$ and $b = 0.3$.

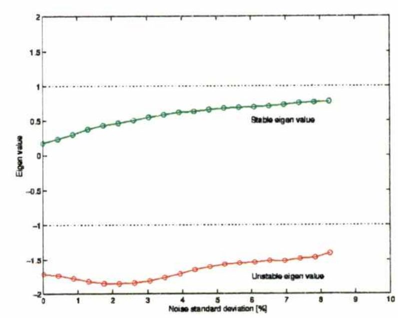


(f) Eigenvalues for $\hat{a} = 1.15$ and $b = 0.3$.

Figure 2.5: Hénon manifold location as a function of Gaussian noise.

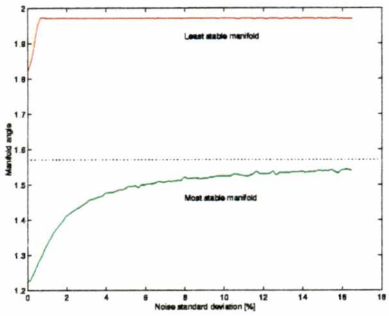


(a) Manifolds for $\hat{B} = 0.30$.

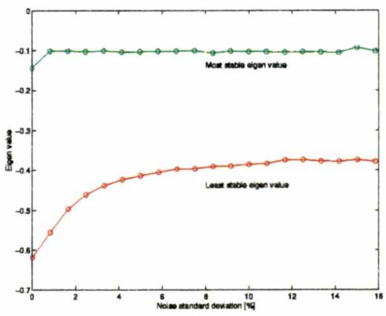


(b) Eigenvalues for $\hat{B} = 0.30$.

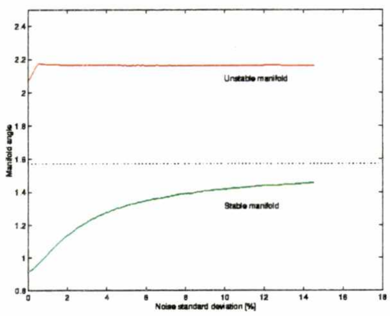


(c) Manifolds for $\hat{B} = 0.55$.

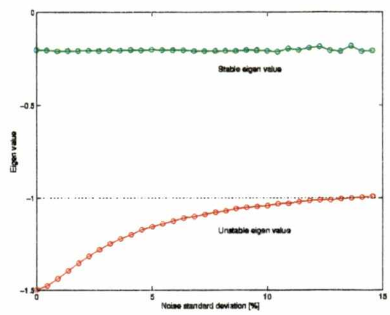


(d) Eigenvalues for $\hat{B} = 0.55$.

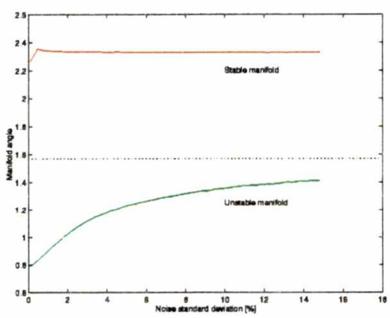


(e) Manifolds for $\hat{B} = 0.76$.

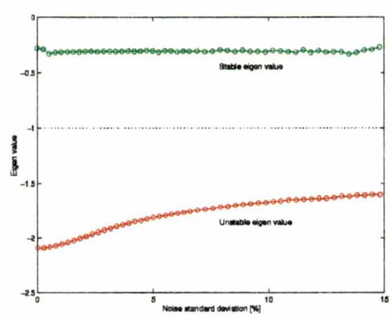


(f) Eigenvalues for $\hat{a} = 0.76$.

Figure 2.6: Ikeda manifold location and eigenvalues as a function of Gaussian noise.

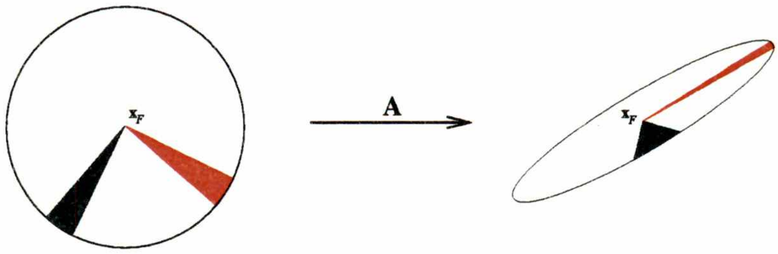


Figure 2.7: The wedges with minimum and maximum expansion after the mapping are orthogonal, and correspond to a set of orthogonal wedges prior to the mapping.

## 2.5 Singular value decomposition

### 2.5.1 Concepts

The eigenvalues and eigenvectors are defined as the expansion factors and directions associated with those directions that do not rotate under the influence of the mapping $\mathbf{M}$. From a geometric viewpoint, it might make more sense to observe and study the expansion factors and directions associated with minimum and maximum expansion. This is illustrated in figure 2.7.

These directions and expansion factors are defined in mathematics as the *singular value decomposition* (SVD) of the mapping $\mathbf{M}$:

$$\mathbf{A} = \mathbf{U}\Sigma\mathbf{V}^T \tag{2.3}$$

Where $\mathbf{U}$ and $\mathbf{V}$ are orthonormal matrices and $\Sigma$ is a diagonal matrix with the *singular values* on the diagonal.

Defining $\mathbf{v}_1$ and $\mathbf{v}_2$ as the vectors — of unit length — along the major and minor axes of the ellipse in figure 2.7 respectively, then $\mathbf{u}_1$ and $\mathbf{u}_2$ are the corresponding vectors before the mapping. Also defined are $\sigma_1$ and $\sigma_2$, which are the scaling factors with $\sigma_1 \geq \sigma_2$.

$$\mathbf{A} = \begin{bmatrix} | & | \\ \mathbf{u}_1 & \mathbf{u}_2 \\ | & | \end{bmatrix} \begin{bmatrix} \sigma_1 & 0 \\ 0 & \sigma_2 \end{bmatrix} \begin{bmatrix} - & \mathbf{v}_1^T & - \\ - & \mathbf{v}_2^T & - \end{bmatrix} \tag{2.4}$$

### 2.5.2 Estimation of U, $\Sigma$, and V

Estimation of the SVD around a fixed point is fairly straight forward using geometric methods based on figure 2.7. The algorithm used picks a large number of random points (uniformly distributed) inside a small wedge at angle $\alpha$ in a small circle around the fixed point and applies the mapping function to all these random points, which results in a wedge in an ellipse, as shown in figure 2.7. The algorithm determines the expansion factor $\sigma'$ for that $\alpha$ by calculating $\sigma'$ for a full rotation of angles $\alpha$ results in a graph as shown in figure 2.8.

The direction of minimum expansion (or maximum contraction) is found by finding that $\alpha$ for which $\sigma'$ is minimized. This minimization finds $\mathbf{u}_2$, $\sigma_2$, and $\mathbf{v}_2$. For a two dimensional space, the other values are then easily determined, since $\mathbf{U}$, and $\mathbf{V}$ must be orthonormal.

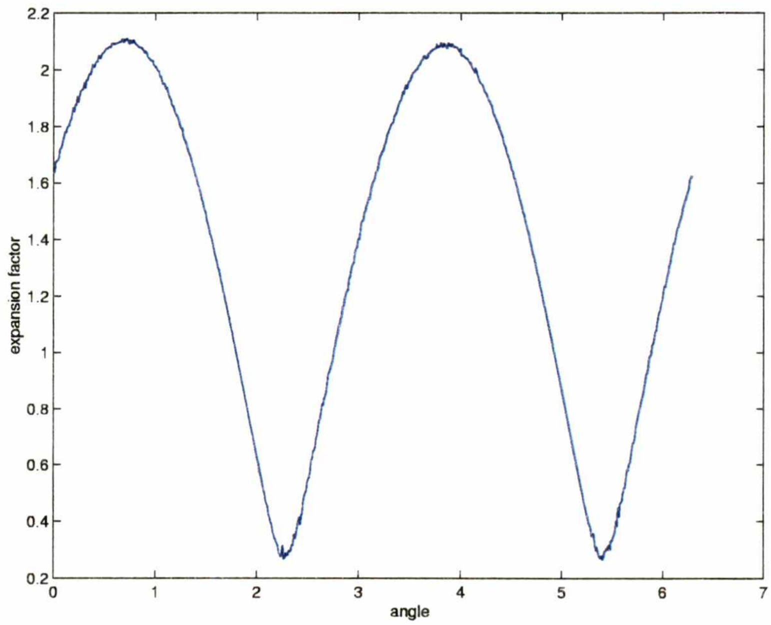


Figure 2.8: Example of a $\sigma'$ plot as function of angle $\alpha$. This particular graph is of the Ikeda map, with noise standard deviation 0.05.

### 2.5.3 Singular direction shifting under the influence of Gaussian noise

As with the eigenvectors, the singular directions were calculated for different noise levels to determine how these directions are influenced by dynamic noise. The numerical experiments were done for the Hénon map, as well as, the Ikeda map, each at several different parameter settings. The results are shown in figure 2.9.

It appears that the singular directions remain constant, even under the influence of noise. This is an important result, since it implies that a control system based on the SVD could possibly be much more robust under the influence of noise than a control system based on eigenvectors and eigenvalues.

## 2.6 Experimental

All experiments done in this chapter were conducted using original C and C++ code. A number of algorithms by Press, Teukolsky, Vetterling, and Flannery (1992) were also used for generation of pseudo-random numbers and for minimization of certain functions. The number of data points varied from $10^5$ for the fixed point determinations to $10^6$ for SVD estimations. Computation were done on both Intel based computers as well as Sun Microstations.

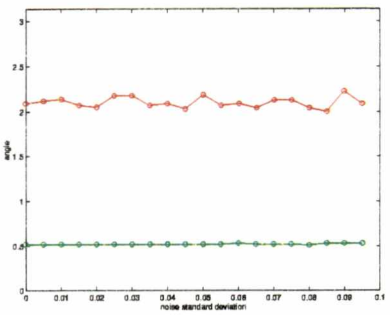

(a) Hénon, period one

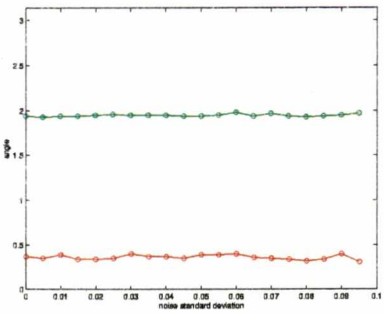

(b) Ikeda, period one

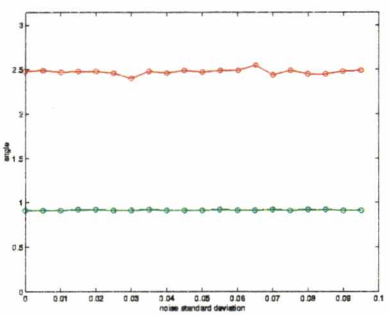

(c) Hénon, period two

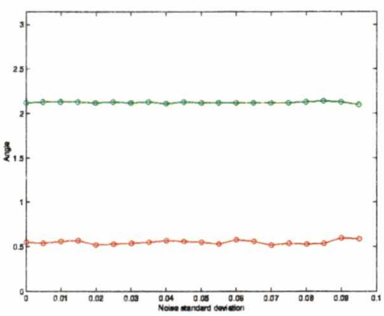

(d) Ikeda, period two

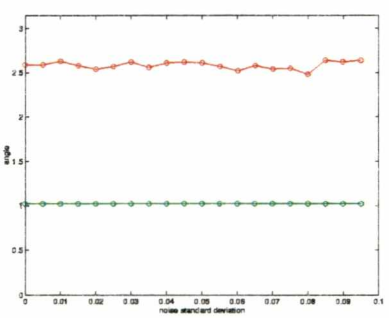

(e) Hénon, chaos

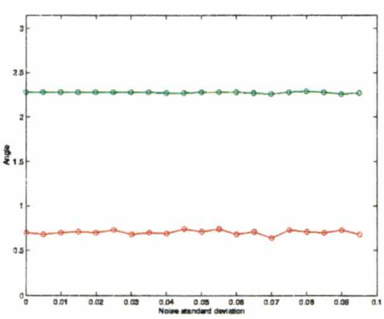

(f) Ikeda, chaos

Figure 2.9: Angles of minimum (green) and maximum (red) expansion of the Hénon and Ikeda maps at different levels of noise. 1000000 random data points were used per wedge.

## 2.7 Summary

In this chapter, new definitions were proposed for a number of dynamic structure concepts in the presence of dynamic noise. Specificly, the fixed point, the manifold structure, the eigenvalues, and the singular value decomposition were defined for systems that are influenced by noise.

Each of the definitions was shown to coincide with the classical definitions of each concept as the noise level approached the limit of zero. It was also shown that several of the concepts do vary with different levels of noise influencing the system (manifold structure and eigenvalues), while others appear to remain unaffected (fixed point and singular value decomposition).

# Chapter 3

# Control concepts

## 3.1 Control index

To determine whether or not a certain control method is effective, an objective index that can be universally evaluated must be defined. The objective of the control algorithms that are being examined is to control the system to a fixed point. When no noise is present, it is assumed that all studied algorithms achieve this control. However, as noise is added, the system will never exactly reach the targeted fixed point. In case of a fairly good control, the system will form a "blob" around the fixed point. The index should be able to distinguish between several different control methods that all perform "fair".

Since the overall control objective is to get onto or as close to the fixed point as possible, one natural control index appears to be taking the average distance of the system from the fixed point, taken over a large number of system iterations.

**Definition 3.1** *Given a certain fixed point* $\mathbf{x}_F$*, and a certain controlled time series* $\mathbf{x}_n$ *with* $n = 1 \cdots N$*, the control index can be defined as*

$$\gamma = \frac{\sum_{n=1}^{N} |(\mathbf{x}_n - \mathbf{x}_F)|}{N} \qquad (N \gg 1)$$

For a controlled system without noise, we should have $\gamma = 0$.

## 3.2 OGY control

To study the effectiveness of the OGY method for a system under the influence of noise, several numerical experiments were done with the Hénon map. The control vector was calculated analytically from the noise-free system. Controlled time series were obtained for this system. For each time series the system was subject to an increased level of noise. For each time series $\gamma$ was calculated. The results are shown in figure 3.1.

As expected, $\gamma$ increases with increased noise level. Note that between $\sigma = 0.06$ and $\sigma = 0.08$, for $\hat{a} = 0.80$, the control index jumps an order of magnitude higher. This is caused by the fact that the OGY control algorithm cannot keep the system within the control circle. The control circle was chosen as large as possible without causing the system to "blow up". If control were engaged outside of this circle, the system would become unstable

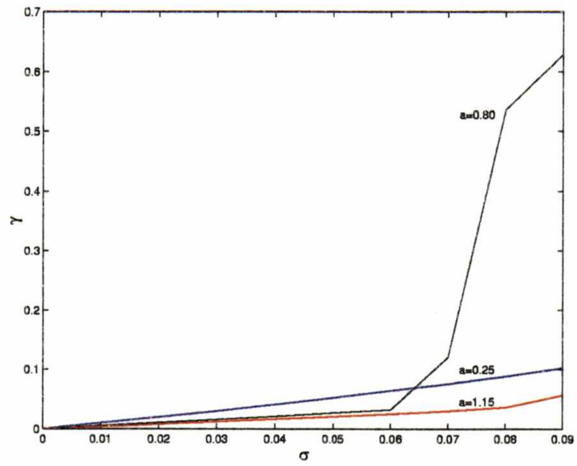


Figure 3.1: Effectiveness of the OGY control method for the Hénon map. The control index $\gamma$ increases as the noise level $\sigma$ is increased for the Hénon map. Each data point was calculated for a time series of length 20000.

and quickly grow to infinity. Once the system escapes the circle, the control was turned off. At this point the system wanders around until it returns to the control circle on its own, at which point the control engages again. Note that this was only the case for the Hénon map. For all other systems, the control was left on at all times. An analogous experiment was done for the Ikeda map. The results are plotted in figure 3.2. The results are qualitatively the same.

## 3.3 SVD control

Derivation of an SVD analog to the OGY control method discussed in section 1.3.1 is fairly straight forward. In fact, it is identical to the OGY deriva-

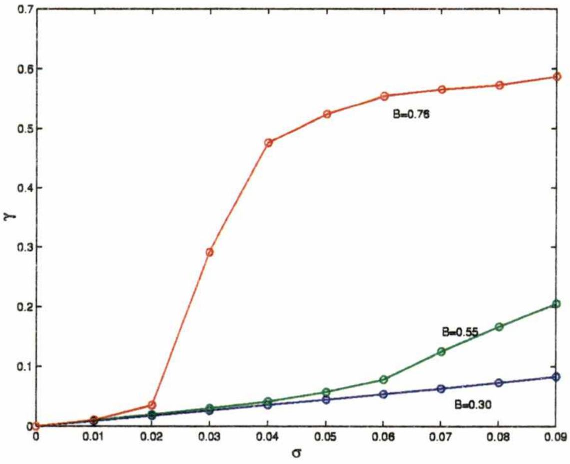


Figure 3.2: Effectiveness of the OGY control method for the Ikeda map. The control index $\gamma$ increases as the noise level $\sigma$ is increased for the Ikeda map. Each data point was calculated for a time series of length 20000.

tion up until the control condition (1.10), which in OGY aims to put the next iterate onto the stable manifold. In the SVD based method, the objective is to place the next iterate onto the direction of maximum contraction. Analogous to the OGY condition, this means that $(\mathbf{x}_{n+1} - \mathbf{x}_F)$ is orthogonal to the direction of maximum expansion, since $\mathbf{U}$ is orthogonal:

$$\mathbf{u}_1^T(\mathbf{x}_{n+1} - \mathbf{x}_F(p)) \tag{3.1}$$

Combining the above equation with (1.9) we obtain

$$\mathbf{u}_1^T\mathbf{J}(\mathbf{x}_n - \mathbf{x}_F(p) - \mathbf{s}\Delta p)\mathbf{u}_1^T\mathbf{s}\Delta p = 0 \tag{3.2}$$

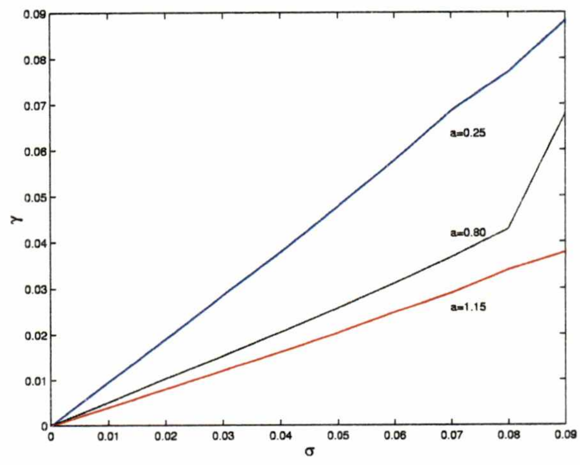


Figure 3.3: Effectiveness of the SVD control method for the Hénon map. The control index $\gamma$ increases as the noise level $\sigma$ is increased for the Hénon map. Each data point was calculated for a time series of length 20000.

Solving for $\Delta p$, we obtain

$$\Delta p = \frac{\mathbf{u}_1^T \mathbf{J} \Delta \mathbf{x}_n}{\mathbf{u}_1^T \mathbf{J} \mathbf{s} - \mathbf{u}_1^T \mathbf{s}} \tag{3.3}$$

As with the OGY method, this results in a simple vector inner product, which is to be applied with every iteration.

The effectiveness of this control method under the influence of noise was tested in the same way as for the OGY method. The results are plotted in figures 3.3 and 3.4 for the Hénon and Ikeda maps respectively.

Overall, the SVD method appears better that the OGY method for the Hénon map, but the two methods are almost indistinguishable for the Ikeda map. Though the number of data points is hardly conclusive, the current evidence suggests the use of the SVD method over the original OGY method,

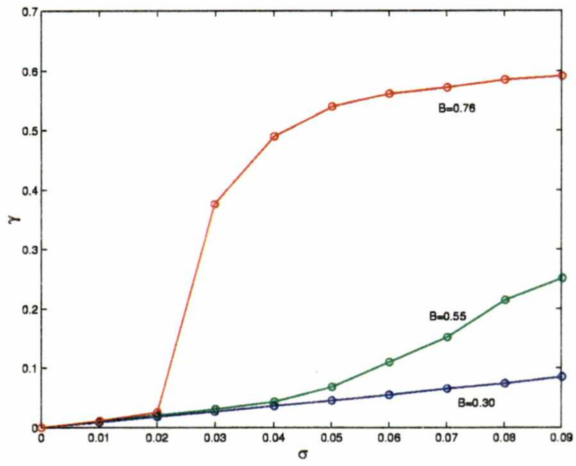


Figure 3.4: Effectiveness of the SVD control method for the Ikeda map. The control index $\gamma$ increases as the noise level $\sigma$ is increased for the Ikeda map. Each data point was calculated for a time series of length 20000.

since the SVD method does not appear worse in any case, and better in some.

## 3.4 Optimal control

Both OGY and SVD control methods are of the form

$$\Delta p = \begin{bmatrix} c_0 & c_1 \end{bmatrix} \begin{bmatrix} \Delta x_0 \\ \Delta x_1 \end{bmatrix} \tag{3.4}$$

where $c_0$ and $c_1$ are determined by the specific control method. Romeiras et.al. (1992), derive the theoretical condition which needs to be met if the controlled system is to converge. This is done by first deriving the mapping function for the controlled system:

$$\mathbf{x}_{n+1} - \mathbf{x}_F = (\mathbf{J} - \mathbf{b}\mathbf{c}^T)(\mathbf{x}_n - \mathbf{x}_F) \tag{3.5}$$

where $\mathbf{J}$ is the Jacobian of the system, $\mathbf{b}$ is the parameter Jacobian ($\frac{\partial \mathbf{F}}{\partial p}$), and $\mathbf{c}$ is the control vector. From this, it then follows that the controlled system will converge to the fixed point if:

$$\lim_{n \to \infty} (\mathbf{J} - \mathbf{b}\mathbf{c}^T)^n = \mathbf{0} \tag{3.6}$$

In other words, this means that the absolutes of all eigenvalues of the matrix $(\mathbf{J} - \mathbf{b}\mathbf{c}^T)$ need to be smaller than one. The control vector $\mathbf{c}$ is the variable in (3.6), and its elements can be used as coordinates on a plane (for 2d systems). Using (3.6), a region in the plane can be specified which designates whether or not the controlled system is theoretically stable. This region is bounded by the following lines of marginal stability (in the two dimensional case):

$$\lambda_1 = \pm 1 \qquad \text{and} \qquad \lambda_1 \lambda_2 = 1 \tag{3.7}$$

These boundaries enclose a triangle within which the controlled system converges. An example for the Hénon map is shown in figure 3.5.

In a practical sense, where observations are made of systems influenced by dynamic noise, it is interesting to assign a control effectiveness $\gamma$ to each

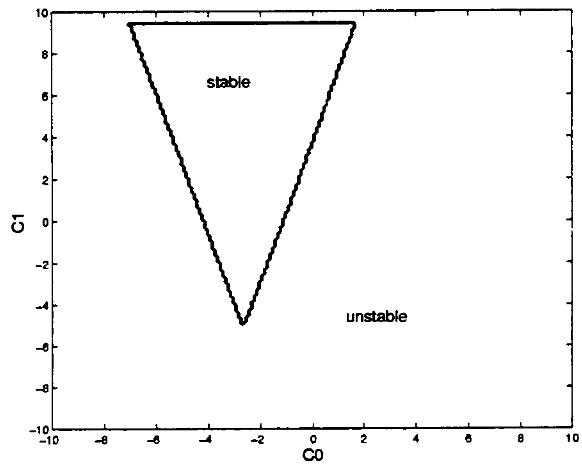


Figure 3.5: Analytically derived stable and unstable regions for the controlled Hénon map.

control vector **c**. It follows then that a surface can be plotted in $< c_0 - c_1 - \gamma >$-space. The control will be optimal (as specified by definition 3.1) when $\gamma$ reaches the surface minimum. The $\gamma$-surface was constructed for a number of systems under the influence of different levels of noise.

### 3.4.1 Optimal Hénon control

The $\gamma$-surface was calculated for the Hénon map at several noise levels, as well as several parameter settings. Figure 3.6 shows the surface for the noisy period one case. To get a better view, most plots are drawn as color coded contour maps.

In each plot, the theoretical stable area as defined by equation (3.6) is shown by a dashed gray line. Notice that the dark blue areas, which represent the minimum on the surface, fall within the theoretical stable area. "Holes" in

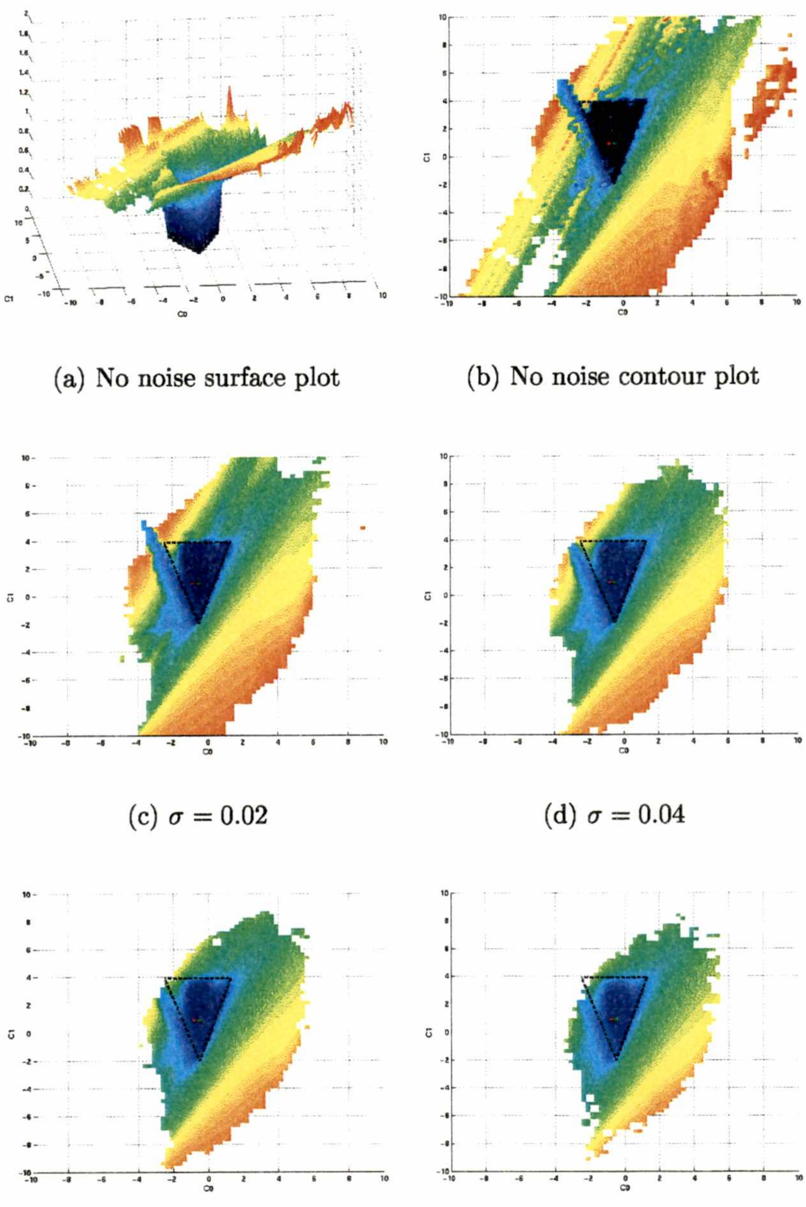

(a) No noise surface plot

(b) No noise contour plot

(c) $\sigma = 0.02$

(d) $\sigma = 0.04$

(e) $\sigma = 0.06$

(f) $\sigma = 0.08$

Figure 3.6: $\gamma$-surfaces for the noisy period one Hénon map. Dark blue indicates good control, while red indicates poor control. In the contour maps the positions of the OGY (red mark) and SVD (green mark) are shown. The gray outline indicates the theoretical stable region.

the surface indicate where the control caused the system to become unstable and unbounded, i.e., the system "blows up." As the noise is increased, the region in which the system remains bounded shrinks. Though the shrinking appears to be asymmetric, the minimum area always remains within the theoretical stable region.

Note that both the OGY and SVD control vector locations (based on noise free analysis) are in the blue region. They are, however, not located in the darkest region, so this indicates that neither of the two are the optimal algorithm. As the noise is increased, the blue area "border" draws closer and closer to both locations. Eventually, as noise continues to increase, control will be lost when OGY and SVD will be located outside of the blue area.

This "loss of control" is in fact demonstrated with the noisy period two parameter setting. These plots are shown in figure 3.7. The SVD method loses control as the blue area shrinks. This is confirmed by the jump in $\gamma$ in figure 3.3. Extrapolating, one expects the OGY method to lose control shortly afterwards. Similar results are also seen for the Hénon system in chaotic motion (figure 3.8).

From these observations the conclusion can be drawn that neither OGY nor SVD control methods are optimal with respect to robustness against dynamic noise, especially in the nominally chaotic region, where the system blows up immediately outside the blue region. Optimally the control vector will be located in a region that remains blue even with very high levels of noise. This is not necessarily the "center" of the blue region or of the

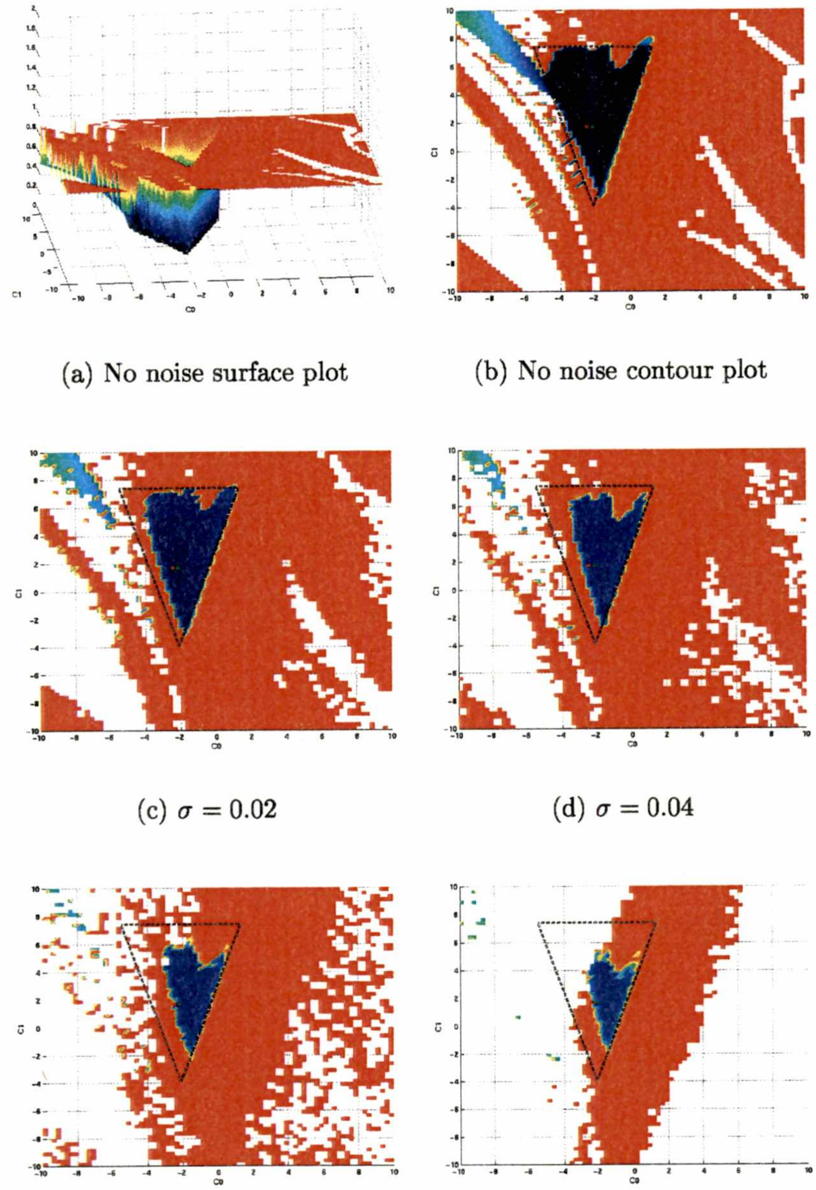

(a) No noise surface plot

(b) No noise contour plot

(c) $\sigma = 0.02$

(d) $\sigma = 0.04$

(e) $\sigma = 0.06$

(f) $\sigma = 0.08$

Figure 3.7: $\gamma$-surfaces for the noisy period two Hénon map. Dark blue indicates good control, while red indicates poor control. In the contour maps the positions of the OGY (red mark) and SVD (green mark) are shown. The gray outline indicates the theoretical stable region.

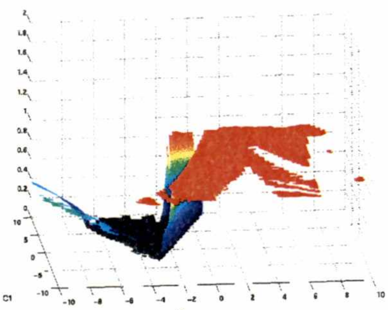

(a) No noise surface plot

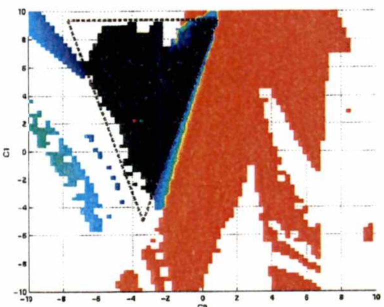

(b) No noise contour plot

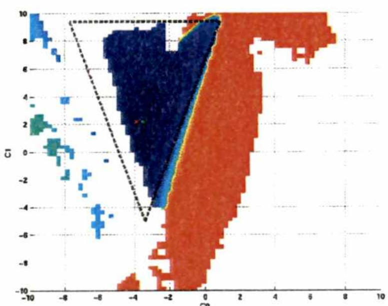

(c) $\sigma = 0.02$

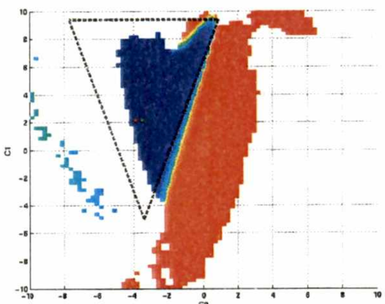

(d) $\sigma = 0.04$

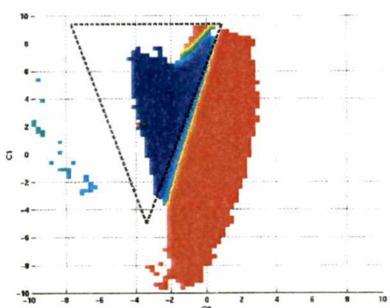

(e) $\sigma = 0.06$

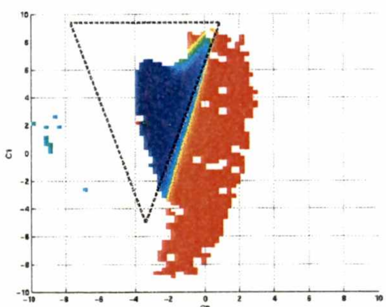

(f) $\sigma = 0.08$

Figure 3.8: $\gamma$-surfaces for the noisy chaotic Hénon map. Dark blue indicates good control, while red indicates poor control. In the contour maps the positions of the OGY (red mark) and SVD (green mark) are shown. The gray outline indicates the theoretical stable region.

theoretical stable region.

### 3.4.2 Optimal Ikeda control

The same experiments were done for the Ikeda map. Because this system does not have the same "blow-up" behavior as the Hénon map, no "holes" are present in the plots (figures 3.9, 3.10 and 3.11). As with the Hénon map, the noise fuzzes out the fractal structure of the surface, and the optimal control region shrinks in a similar manner as with the Hénon map.

## 3.5 Engine control

To examine a model representing an actual physical system, the $\gamma$-surface was determined for a model of an internal combustion engine as describes in section 1.5.2.

When designing a control algorithm for the engine based on the heat release a question arises: how many cycles back in time should be included? If only the current heat release is considered, the control becomes a simple proportional one dimensional control:

$$\Delta p_{i+1} = c(hr_i - hr_F) \tag{3.8}$$

The $\gamma$-surface in this case becomes a line. If we consider $hr_i$ and $hr_{i-1}$, the

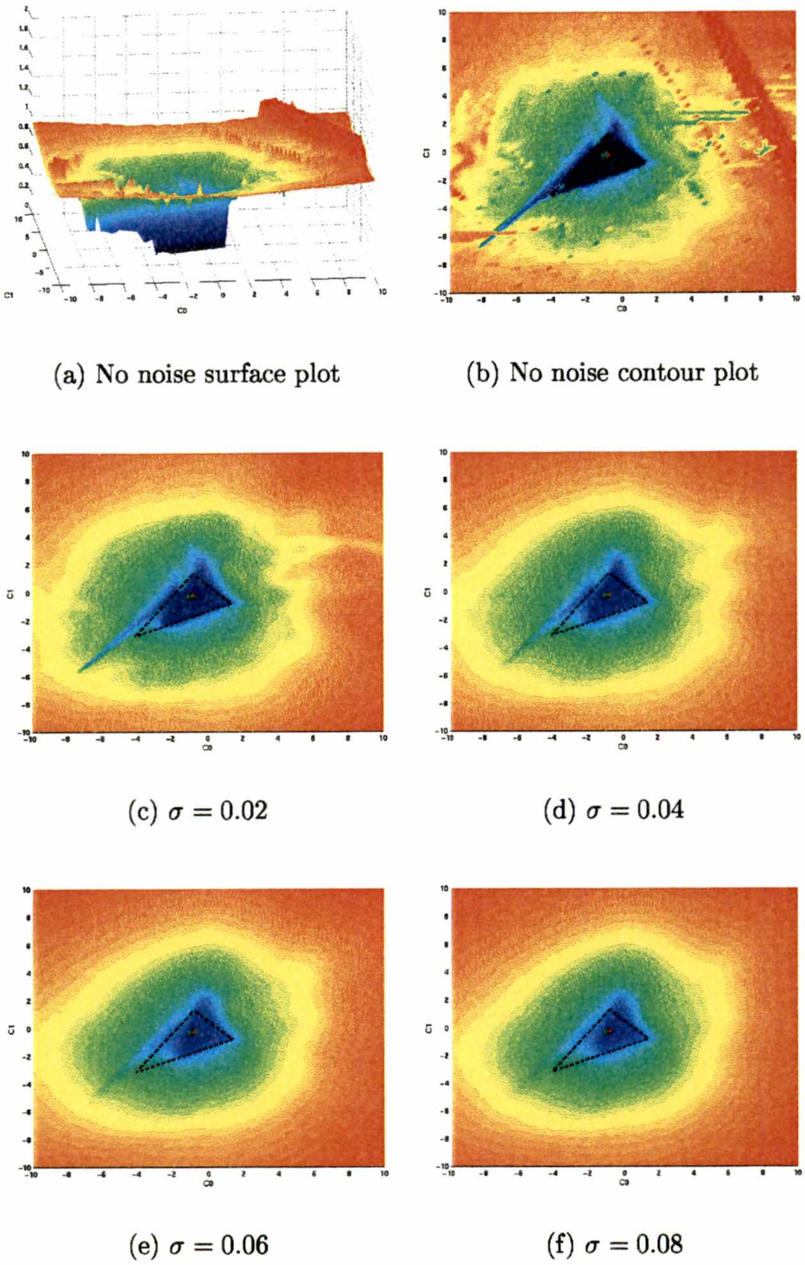

(a) No noise surface plot

(b) No noise contour plot

(c) $\sigma = 0.02$

(d) $\sigma = 0.04$

(e) $\sigma = 0.06$

(f) $\sigma = 0.08$

Figure 3.9: $\gamma$-surfaces for the noisy period one Ikeda map. Dark blue indicates good control, while red indicates poor control. In the contour maps the positions of the OGY (red mark) and SVD (green mark) are shown. The gray outline indicates the theoretical stable region.

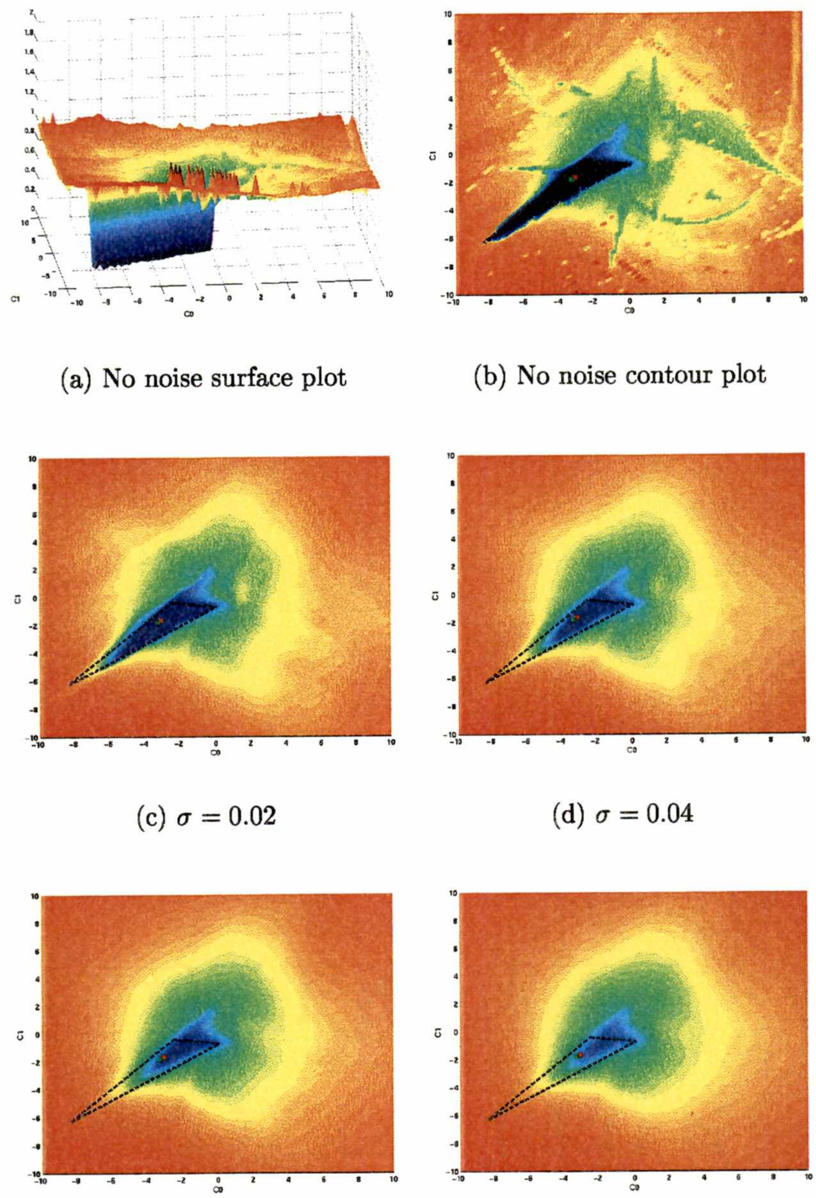

(a) No noise surface plot

(b) No noise contour plot

(c) $\sigma = 0.02$

(d) $\sigma = 0.04$

(e) $\sigma = 0.06$

(f) $\sigma = 0.08$

Figure 3.10: $\gamma$-surfaces for the noisy period two Ikeda map. Dark blue indicates good control, while red indicates poor control. In the contour maps the positions of the OGY (red mark) and SVD (green mark) are shown. The gray outline indicates the theoretical stable region.

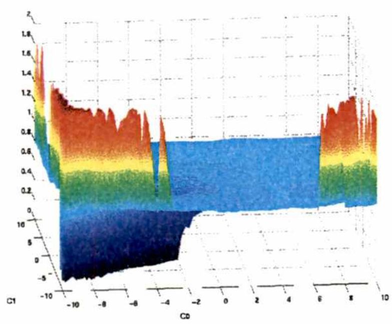

(a) No noise surface plot

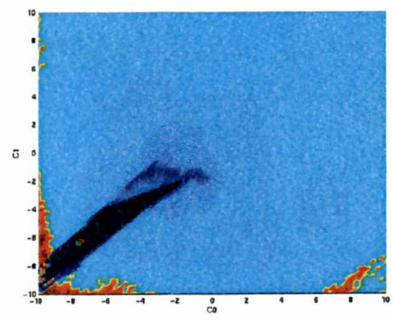

(b) No noise contour plot

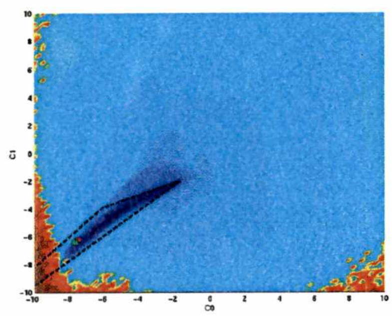

(c) $\sigma = 0.02$

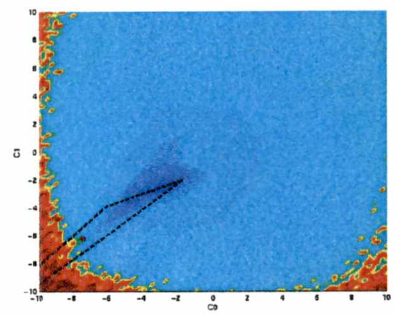

(d) $\sigma = 0.04$

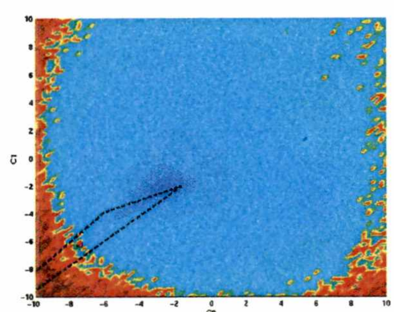

(e) $\sigma = 0.06$

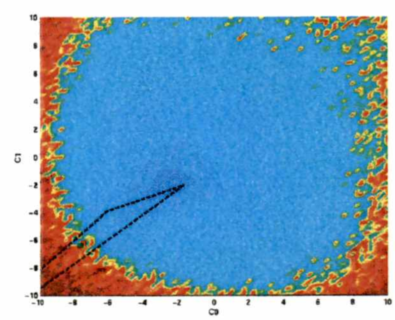

(f) $\sigma = 0.08$

Figure 3.11: $\gamma$-surfaces for the noisy chaotic Ikeda map. Dark blue indicates good control, while red indicates poor control. In the contour maps the positions of the OGY (red mark) and SVD (green mark) are shown. The gray outline indicates the theoretical stable region.

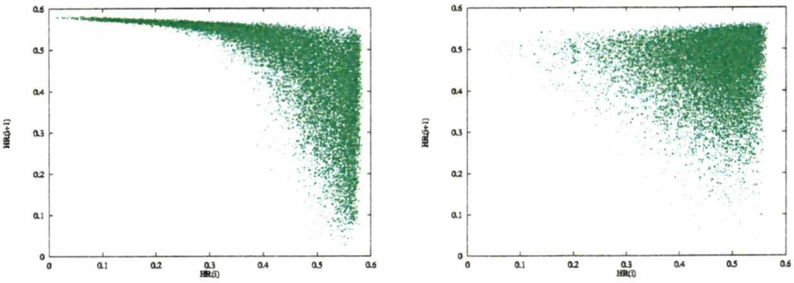

(a) No control (b) Optimal control

Figure 3.12: Heat release return maps for the engine model. These particular parameter settings represent a noisy period two.

control becomes two dimensional as with the Hénon and Ikeda maps:

$$\Delta p_{i+1} = \begin{bmatrix} c_0 & c_1 \end{bmatrix} \times \begin{bmatrix} hr_{i-1} - hr_F \\ hr_i - hr_F \end{bmatrix} \tag{3.9}$$

This can be increased to as many dimensions as desired, but the question is: which is optimal, and where are the returns diminished?

Figure 3.13 shows the one dimensional $\gamma$-surface. It shows that one dimensional control can improve $\gamma$ by a factor of 0.67. A plot of the controlled system is shown in figure 3.12b. Notice, however, that the minimum $\gamma$ lies close to a very steep incline which implicates flame-out. This suggests that if the control would only be slightly off, the result could be catastrophic, i.e., flame-out.

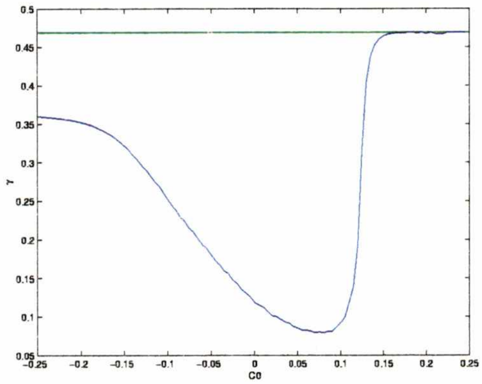


Figure 3.13: One dimensional $\gamma$-surface for the engine model (blue line). The green line indicates the flame-out level.

Figure 3.14 shows the two dimensional $\gamma$-surface. The flame-out "cliff" is very prominent. Also visible is the effective control valley. The valley appears to be very flat. The cross-section $c_0 = 0$ in this surface will result in the one dimensional control plot. Notice how on this line the dark blue region is pressed right up against the flame-out region to its "north". If $c_0$ moves somewhat to the west, we see that the flame-out cliff moves further away and that the dark blue valley extends further to the south. Since the valley is quite flat, it does not matter much where in the valley we are with respect to $\gamma$. However, the robustness of the control improves if $c_0$ is set a little negative.

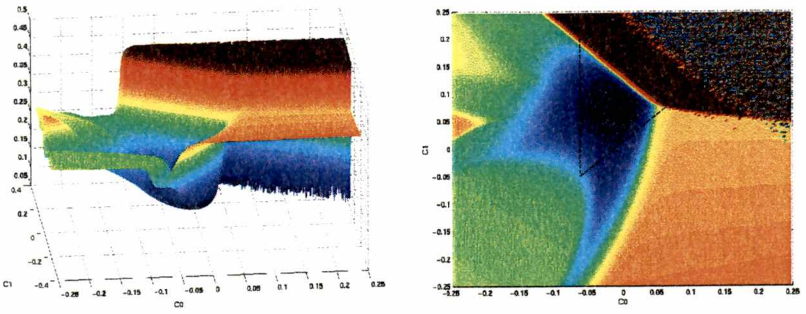

(a) 3d view (b) Top view

Figure 3.14: $\gamma$-surface for the two dimensional control on the noisy engine model.

Figure 3.15 shows a sequence of contour views of how the surface would vary when using three dimensional control. From the figures, there does not appear to be any benefit with respect to robustness to using three dimensional control.

In figure 3.16 the minimum $\gamma$ is shown for some higher dimensions as well. It shows that using higher dimensions improves $\gamma$ only very marginally.

## 3.6 Experimental

All experiments done in this chapter were conducted using original C and C++ code. A number of algorithms by Press, Teukolsky, Vetterling, and Flannery (1992) were also used for generation of pseudo-random numbers and for minimization of certain functions. The number of data points used

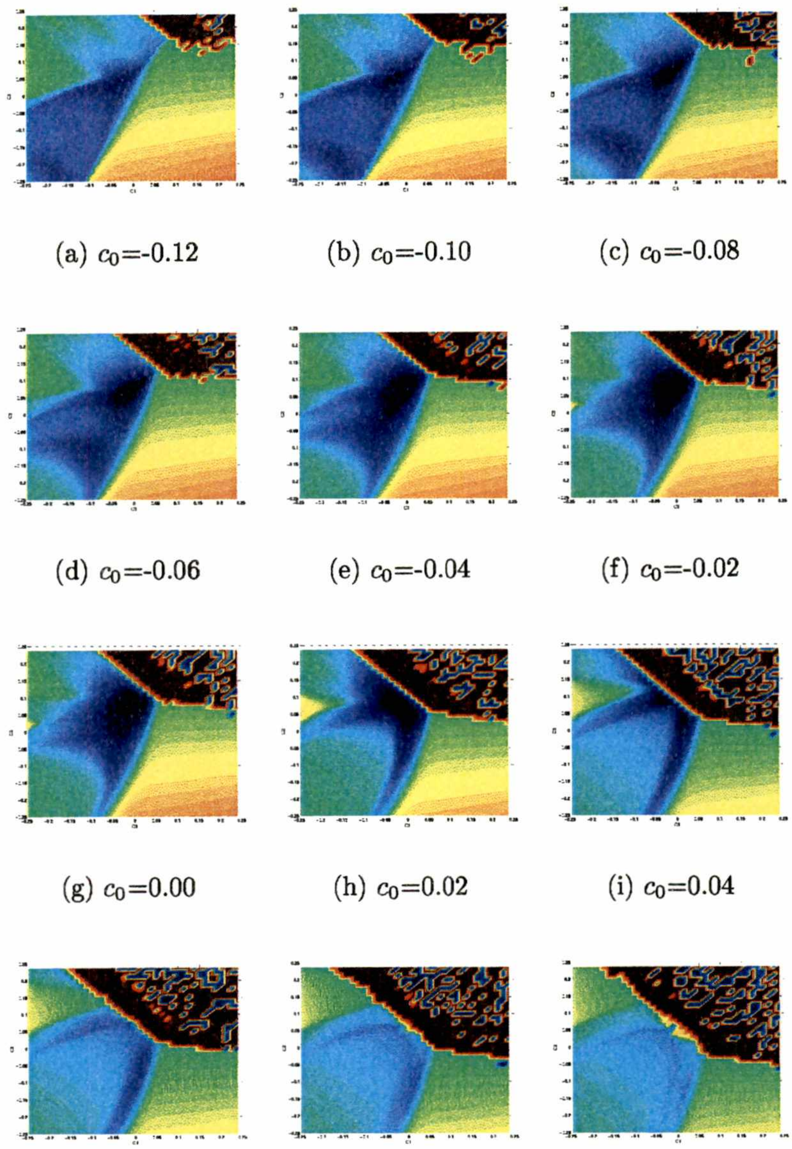

(a) $c_0$=-0.12 (b) $c_0$=-0.10 (c) $c_0$=-0.08

(d) $c_0$=-0.06 (e) $c_0$=-0.04 (f) $c_0$=-0.02

(g) $c_0$=0.00 (h) $c_0$=0.02 (i) $c_0$=0.04

(j) $c_0$=0.06 (k) $c_0$=0.08 (l) $c_0$=0.10

Figure 3.15: Three dimensional control $\gamma$-surfaces for the engine model.

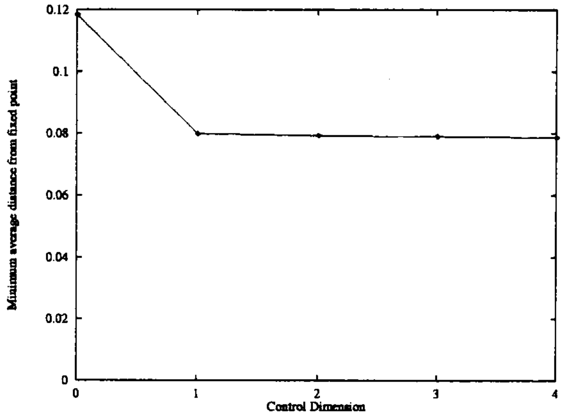


Figure 3.16: Minimum $\gamma$ for several dimensions.

for each control experiments was $2 * 10^4$. Computation were done on both Intel based computers as well as Sun Microstations.

The basic control algorithm left the control on at all times, except for the Hénon map. The Hénon map becomes unstable if control is actuated when the system state is outside the immediate vicinity of the fixed point.

## 3.7 Summary

From the results in this chapter, it is seen that the theoretical stable region defined by equation 3.6 plays an important role in practical situations where the system is influenced by noise. The experimental region of control appears to remain within this theoretical stable area at all times, even though the region of control does contract as noise levels are increased. It is also noteworthy that the contraction does not appear to be uniform in all directions. It seems that the control region hugs the edge closest to the origin.

Both the OGY as well as the SVD control vectors are located within the theoretical stable region, but they are not necessarily within the control region. Thus it follows that neither of these are optimal control vectors when systems are influenced by noise. There does not appear to be any conclusive evidence from these experiments whether or not the SVD method is superior to the OGY method.

As expected, from the engine model experiments it was found that in embedded systems, there is an optimal number of time steps to look back in time. When using higher and higher dimensions, one encounters diminishing returns.

# Chapter 4

# Control optimization

In the previous chapter, a control index was defined, and some experiments were done to examine its behavior for some different systems. It was shown that the control of noisy systems can be optimized by finding the minimum on a surface. Unfortunately, generic minimum finding algorithms are tedious and would require a great number of experiments. This is highly undesirable in an industrial environment, where computation time and the number of experiments needs to be minimized. In this chapter, a number of "rules of thumb" will be investigated which should help the experimentalist minimize the number of experiments needed to find the optimal control point.

## 4.1 Shifting of the OGY control vector due to noise

In chapter 2 it was found that the manifold structure changes as noise is added to the system. These modified manifolds can be used to calculate new control parameters using the OGY formula (1.16). The hypothesis that these new OGY parameters give the optimal control can then be tested.

The parameters were calculated using the data from figures 2.5 and 2.6. The results were plotted on contour maps of the $\gamma$-surface as shown in figure 4.1. The figures show that using the manifold structure as modified by noise does not improve control. The control vector does not move towards the lowest point of the valley as the noise is increased. In some cases (especially the Ikeda map), the control even becomes worse. The contours, however, do show that there appears to be a direction in which the optimal control parameters prefer to move as noise is increased.

## 4.2 Experimental control minima and the theoretical control region

The experimental control minimum can be determined for every noise level and parameter setting from the data collected in chapter 3. It is of interest to study how these minima change as the noise level changes, and how this change relates to the theoretical control region.

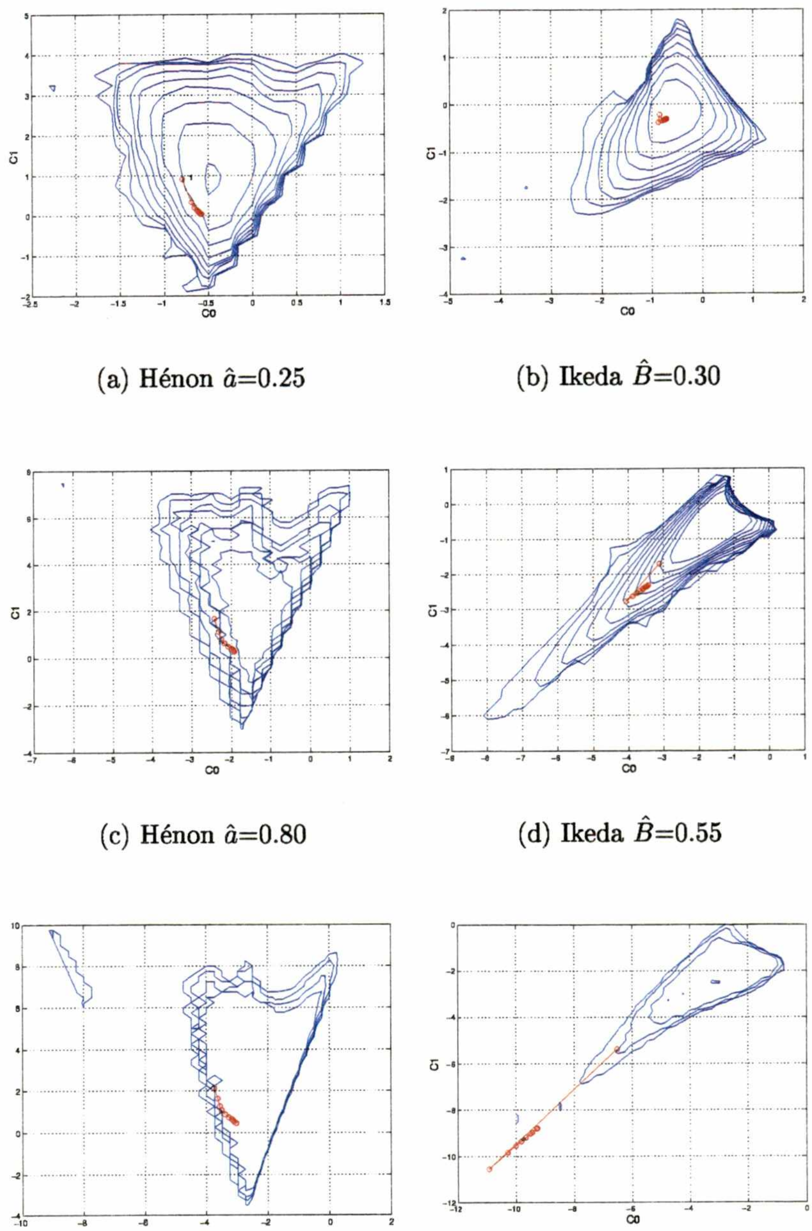

(a) Hénon $\hat{a}$=0.25

(b) Ikeda $\hat{B}$=0.30

(c) Hénon $\hat{a}$=0.80

(d) Ikeda $\hat{B}$=0.55

(e) Hénon $\hat{a}$=1.15

(f) Ikeda $\hat{B}$=0.76

Figure 4.1: Variation of the OGY control vector with increased noise. The blue contours signify equal $\gamma$ values at different noise levels. The inner contours reflect higher noise levels. The red connected circles indicate re-estimated control vector locations for increasing noise levels.

### 4.2.1 Hénon map

The minima for the Hénon map are plotted in figure 4.2. It is apparent that the minimum does not appear to move with increased noise levels. The question that arises is if this location can be derived from (3.5). If so, the optimization effort could be greatly reduced.

In chapter 2 it was discovered that the manifold structure changes with changing noise levels. The fixed point itself, however, remained unaffected by noise. It stands to reason then that a control strategy that projects the next iterate onto this fixed point should be less affected by noise than strategies (such as OGY) that control to the stable manifold. From (3.5) it is easily determined that the system should collapse immediately onto the fixed point when all eigenvalues of the matrix $\mathbf{J} - \mathbf{b}\mathbf{c}^T$ are equal to zero. For the two dimensional case, this condition can be reduced to the solution of the following system:

$$\begin{bmatrix} b_1 & b_2 \\ j_{22}b_1 - j_{12}b_2 & j_{11}b_2 - j_{21}b_1 \end{bmatrix} \mathbf{c} = \begin{bmatrix} \text{trace}(\mathbf{J}) \\ |\mathbf{J}| \end{bmatrix} \tag{4.1}$$

The above system is easily solved for the Hénon system, and the corresponding values for the control vector $\mathbf{c}$ are plotted in figure 4.2. In the figure, the minima are shown as small red dots. The figure shows that there is indeed a very good correspondence between the calculated location and the experimentally determined minima.

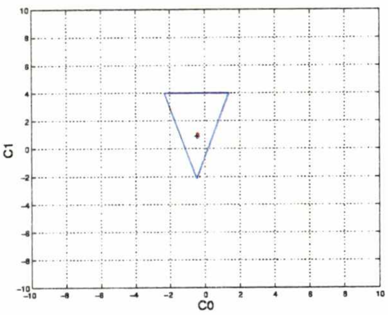


(a) Hénon $\hat{a}$=0.25

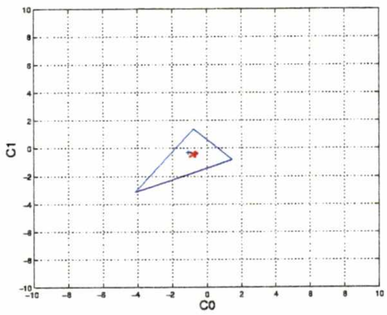


(b) Ikeda $\hat{B}$=0.30

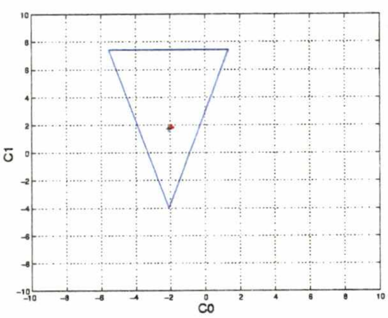


(c) Hénon $\hat{a}$=0.80

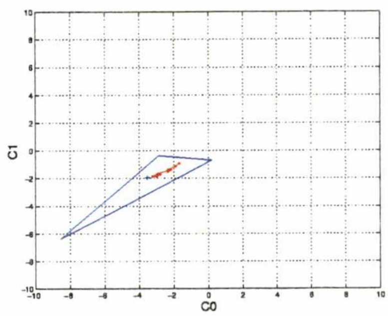


(d) Ikeda $\hat{B}$=0.55

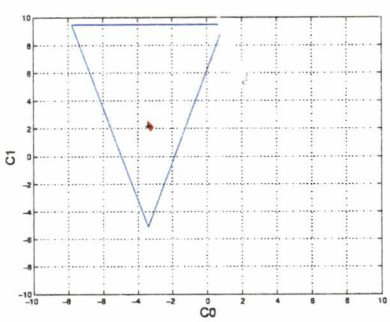


(e) Hénon $\hat{a}$=1.15

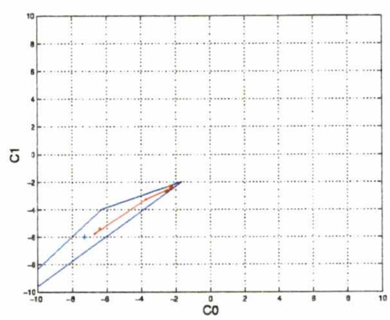


(f) Ikeda $\hat{B}$=0.76

Figure 4.2: Effect of increased noise levels on the minima in the $\gamma$-surface. The minima at different noise levels are indicated by the red dots. The position of the solution to $\lambda_1 = \lambda_2 = 0$ is indicated by the '+' symbol. The triangles indicate the theoretical stable control region.

### 4.2.2 Ikeda map

The same experiments as for the Hénon map were done for the Ikeda map. The results, however, are somewhat different, as figure 4.2 demonstrates. Though the minima remain more or less stationary for different noise levels for the period one system, the minima definitely change for the period two and chaos parameter settings. The trend appears to be that at low noise levels the minimum is close to the control vector as defined by (4.1). When the noise level increases, the minimum drifts towards the origin, which corresponds to no-control. This is consistent with the contours in figure 4.1, where the control region boundary closest to the origin remains least affected by noise levels. Thus a significant observation is that the higher the noise level, the less control action will be desirable.

The discrepancy between Hénon and Ikeda can be explained by the fact that Ikeda is much more sensitive to noise, which causes the system to be dominated by noise more easily. Some slight drift towards the origin can be observed in the Hénon plots, but higher noise levels cannot be examined, since the Hénon map becomes unstable with higher noise levels.

## 4.3 Guidelines

A number of observations can be made when observing the behavior of the location of the optimal control in figure 4.2. The first is that at lower levels of noise, the optimal control vector is located at that position where all eigenvalues of the mapping matrix of the controlled system equal zero. This control vector corresponds to the system immediately collapsing onto the fixed point. This is in contrast to the original OGY control vector, which positions the system onto the stable manifold. That controlling to the fixed point is more effective for noisy systems than controlling to the stable manifold fits with the observations in chapter 2 that the fixed point does not appear to move under the influence of noise, while the manifold structure does change. According to this, a first guideline towards the optimization of control of nonlinear and chaotic systems under the influence of dynamic noise can be stated:

**Guideline 1** *Determine* $\mathbf{J}$ *and* $\mathbf{b}$ *(as defined by (3.5)) of the system from experimental data. Using these, calculate* $\mathbf{c}_o$ *according to the condition that all eigenvalues of* $\mathbf{J} - \mathbf{b}\mathbf{c}_o^{\mathrm{T}}$ *are zero. If noise levels are not expected to be very high, use this* $\mathbf{c}_o$ *as the initial guess for optimal control.*

A second observation is that as noise levels increase, the optimal control migrates towards the origin. As higher noise levels start dominating the system, large control actions disturb the system rather than stabilize it. Thus at higher noise levels, less perturbation is favored. Note, however, that the minimum never leaves the area defined as the stable region. This is also apparent from figure 4.1, where the higher noise contours always remain inside lower noise contours. It is also clear from figure 4.1 that the area edge closest to the origin remains least perturbed by noise. A second guideline

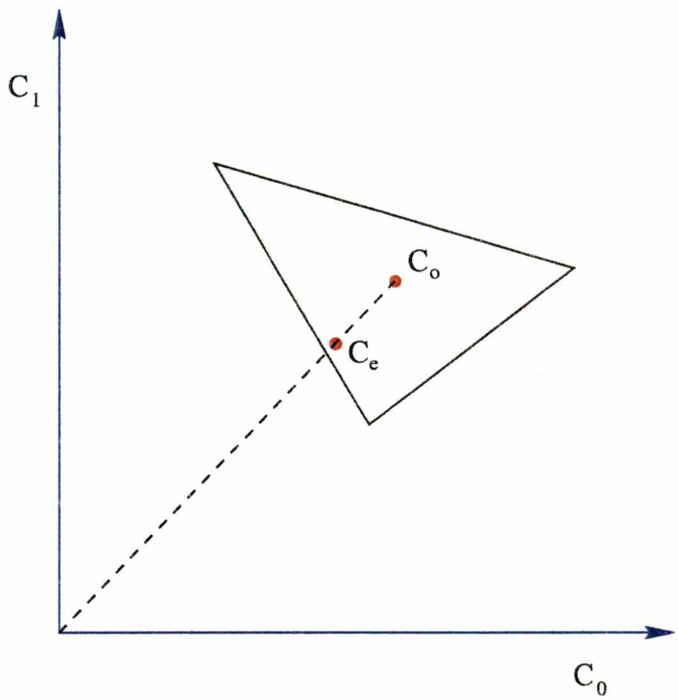


Figure 4.3: Location of $\mathbf{c}_o$ and $\mathbf{c}_e$ for an imaginary system.

can be derived from these observations.

**Guideline 2** *In case of high noise, having determined* $\mathbf{c}_o$ *and the theoretical stable region, draw a line between* $\mathbf{c}_o$ *and the origin of the control space. Locate the intersection between this line and the edge of the stable region closest to the origin. Use the control vector* $\mathbf{c}_e$*, which is located a little on the inside of the stable region from the intersection, as the initial guess.*

Figure 4.3 illustrates the locations of $\mathbf{c}_o$ and $\mathbf{c}_e$. The line connecting $c_o$ and the origin can be expressed in the following equation:

$$c_l = \alpha c_o \tag{4.2}$$

where $c_l$ is any point on the line, and $\alpha$ is the variable. To limit the line to the line section between $c_o$ and $c_e$, a range must be given for $\alpha$. The upper limit for $\alpha$ is easily recognized as $\alpha_o \leq 1$. The lower limit depends on which of the three conditions defined in (3.7) results in the stable area edge between the origin and $c_o$. Equations $\alpha$ for each of the three conditions are as follows:

$$\begin{aligned}
\lambda_1 = 1 \qquad & \alpha_e = \frac{-1 - |\mathbf{J}| + \mathrm{Tr}(\mathbf{J})}{(j_{12}b_2 - j_{22}b_1)c_{o0} + (j_{21}b_1 - j_{11}b_2)c_{o1} + (b_1c_{o0} + b_2c_{o1})} \\
\lambda_1 = -1 \qquad & \alpha_e = \frac{-1 - |\mathbf{J}| - \mathrm{Tr}(\mathbf{J})}{(j_{12}b_2 - j_{22}b_1)c_{o0} + (j_{21}b_1 - j_{11}b_2)c_{o1} - (b_1c_{o0} + b_2c_{o1})} \\
\lambda_1 * \lambda_2 = 1 \qquad & \alpha_e = \frac{1 - |\mathbf{J}|}{(j_{12}b_2 - j_{22}b_1)c_{o0} + (j_{21}b_1 - j_{11}b_2)c_{o1}}
\end{aligned}$$

Once the appropriate $\alpha_e$ has been determined, a third guideline follows:

**Guideline 3** *Search for the control minimum on the line connecting* $\mathbf{c}_o$ *and* $\mathbf{c}_e$*. This line will be defined by (4.2) with* $\alpha_e < \alpha \leq 1$*.*

## 4.4 Optimal Engine Control

The guidelines developed in the previous section were first tested on the engine model. For this model the actual optimal control can be determined by finding the minimum on the $\gamma$-surface in figure 3.14. This minimum was identified to the closest grid point on the surface as:

$$\mathbf{c}_m \approx \begin{bmatrix} -0.01 \\ 0.075 \end{bmatrix}$$

The task is to see if we can approximate $\mathbf{c}_m$ using the above mentioned guidelines.

The nominal values for $\mathbf{J}$ and $\mathbf{b}$ can be determined from the noiseless model in a straightforward manner. Due to the fact that the data is observed as a return map, both $\mathbf{J}$ and $\mathbf{b}$ will be sparse:

$$\mathbf{J}_n = \begin{bmatrix} 0 & 1 \\ 0 & -1.188 \end{bmatrix} \qquad \mathbf{b}_n = \begin{bmatrix} 0 \\ -15.9 \end{bmatrix}$$

In a true experiment, only a time series of the system will be available, so this must be used to determine $\mathbf{J}$ and $\mathbf{b}$ empirically. This estimation was done by observing the time series from the model and recording a large number of data points that fell close to the fixed point. Once a sufficiently large number of data points was collected (approximately $10^5$ cycles), $\mathbf{J}$ was estimated by fitting the equation

$$\begin{bmatrix} h_{n+1} \\ h_{n+2} \end{bmatrix} = \mathbf{J} \begin{bmatrix} h_n \\ h_{n+1} \end{bmatrix}$$

to the data. $\mathbf{b}$ was estimated by determining $\frac{\partial h_{n+1}}{\partial B}|_{h=h_f}$ from a second time series where the parameter $B$ had been perturbed slightly. The derivative is then estimated as:

$$\left.\frac{\partial h_{n+1}}{\partial B}\right|_{h=h_f} \approx \left.\frac{\overline{h_{n+1}(B+\Delta B) - h_{n+1}(B)}}{\Delta B}\right|_{h=h_f} = \frac{\overline{h_{n+1}(B+\Delta B)}|_{h=h_f} - h_f}{\Delta B}$$

where the overbar refers to the average value. Using these methods, $\mathbf{J}$ and $\mathbf{b}$ were determined:

$$\mathbf{J} = \begin{bmatrix} 0 & 1 \\ 0.13 & -1.33 \end{bmatrix} \qquad \mathbf{b} = \begin{bmatrix} 0 \\ -14.7 \end{bmatrix}$$

Note that both $\mathbf{J}$ and $\mathbf{b}$ were determined without doing any control on the system. Only two time series are in principle necessary, though a large number of cycles might be called for. For very noisy systems, it might be desirable to acquire more data sets to estimate $\mathbf{b}$. Each data set would have a slightly different parameter perturbation, so as to get a more accurate estimation. Now, equation (4.1) can be solved for the empirical values to find $\mathbf{c}$:

$$\mathbf{c}_o = \begin{bmatrix} -0.009 \\ 0.091 \end{bmatrix}$$

In figure 4.4 both $\mathbf{c}_m$ and $\mathbf{c}_{est}$ are plotted on the control plane. Note that $\mathbf{c}_{est}$ is close to $\mathbf{c}_m$, and is also close to the line connecting $\mathbf{c}_{est}$ and the origin. This is a first confirmation of the guidelines developed in the previous section.

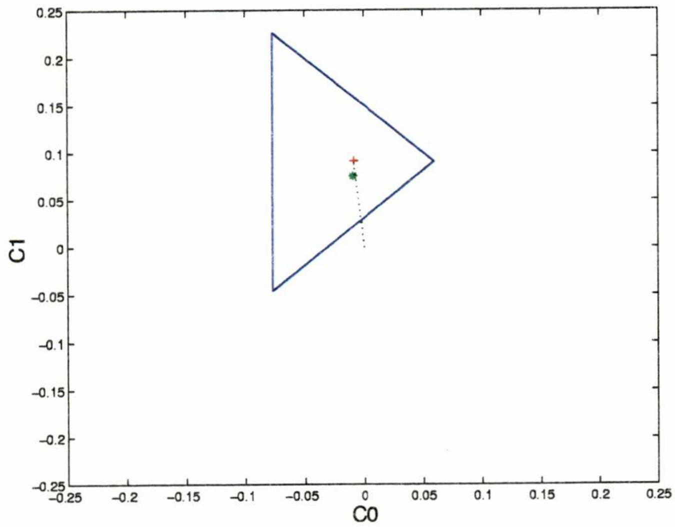


Figure 4.4: Location of $\mathbf{c}_m$ (green $*$) and $\mathbf{c}_o$ (red $+$) on the control plane.

# 4.5 Control of the CSTR model

## 4.5.1 OGY control without added noise

The fixed point on the Poincaré section was located and determined to be

$$y_f = \begin{bmatrix} 0.531 \\ 0.799 \end{bmatrix}$$

Using equation (1.16) the OGY control vector was calculated,

$$c_{\mathrm{OGY}} = \begin{bmatrix} 0.562 \\ 0.0820 \end{bmatrix}$$

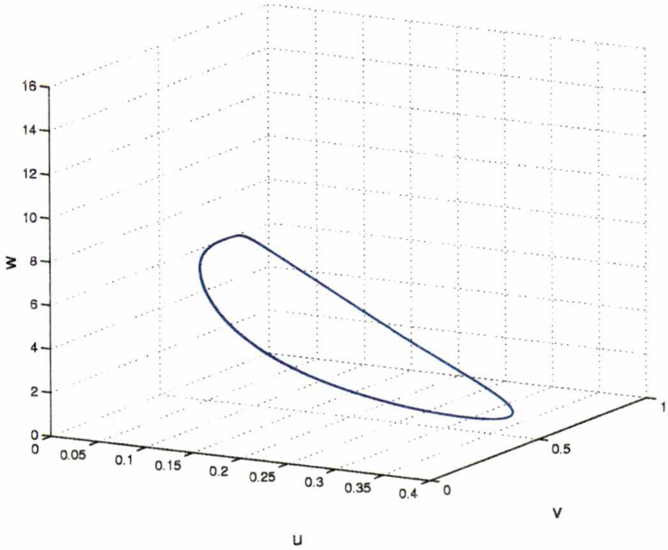


Figure 4.5: OGY controlled CSTR without added noise.

and this vector was used to control the system to a period one oscillation. The result is shown in figure 4.5.

### 4.5.2 Control of the CSTR model with added noise

As with the other models, a $\gamma$-surface was constructed for the noisy CSTR model. Due to prohibitive calculation times, the number of points on the $< c_0 - c_1 >$-plane could not be very large. Also, the number of cycles had to remain relatively low (500 per grid point). As a result, the $\gamma$-surface cannot be very detailed, though general trends can be deduced. The plot of the figure is shown in figure 4.6. The estimated $\mathbf{c}_o$, $\mathbf{c}_{\min}$, and relevant edge of the theoretical stable area are also shown in the plot. Notice that the edge passes right above the origin, which confirms that the fixed point

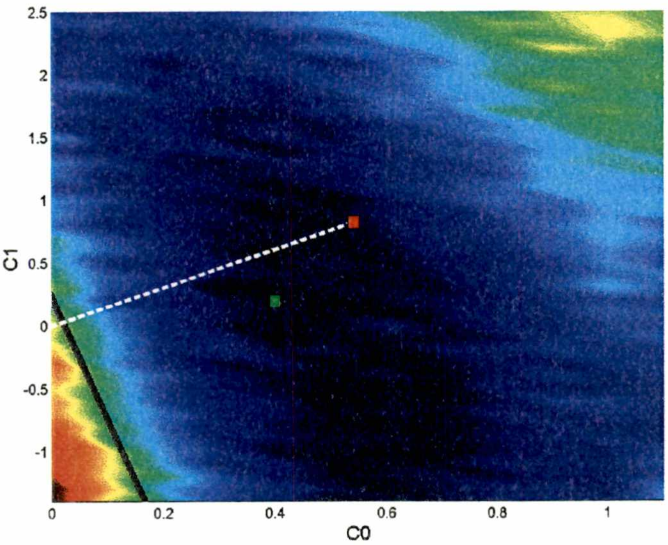


Figure 4.6: $\gamma$-surface of the noisy CSTR model. The grey diagonal shows the line corresponding to $\lambda_1 = -1$. The red point indicates the estimated location of $\mathbf{c}_o$. The green point gives a rough estimate of the minimum on the $\gamma$-surface. The white dashed line connects $\mathbf{c}_o$ and the origin.

is only barely unstable on its own. The other edges of the theoretical stable area stretch out beyond the right and top edges of figure 4.6. The Poincaré section of the system controlled with the minimum control vector is shown in figure 4.7.

Once again it appears that the control region remains within the theoretical stability region when noise is added. Because of the inaccuracy in the determination of $\mathbf{J}$ and $\mathbf{b}$, caused by the lack of a great amount of data points, it cannot be expected that the guidelines hold exactly. Given this, figure 4.6 shows that $\mathbf{c}_{\min}$ does fall roughly between $\mathbf{c}_o$ and the origin, even though it is not on or very close to the dashed white line in the figure. The experiments do confirm that when using the guidelines given, one would come

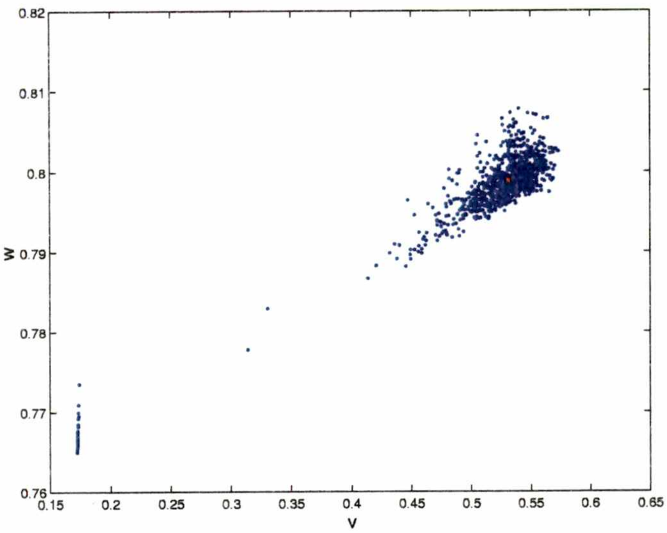


Figure 4.7: Poincaré section of the system controlled with $\mathbf{c}_{\min}$

fairly close to the optimal control point.

## 4.6 Experimental

All Hénon, Ikeda, and engine experiments done in this chapter were conducted using original C and C++ code. A number of algorithms by Press, Teukolsky, Vetterling, and Flannery (1992) were also used for generation of pseudo-random numbers. Integration of the CSTR model was done using Matlab 5.1 routine `ode15s` on Intel based computers.

## 4.7 Summary

In this chapter a number of guidelines to find the optimal control vector were developed by observation of the behavior of the Hénon and Ikeda maps. These rules of thumb intend to optimize the search for the best control (as defined by definition 3.1). The guidelines were tested on two realistic models. It was found that the guidelines do aid in the determination of the optimal control, though a large number of data points is desirable when dealing with considerable noise levels.

# Chapter 5

# Conclusion

The main objective of this research has been to develop a modified version of the original OGY control method so as to optimize control of nonlinear and chaotic system influenced by dynamic noise. Specifically, the objective of the control algorithms is to stabilize periodic orbits in phase space. The research was conducted by studying three conjectures (section 1.5.1).

## 5.1 Concerning Conjecture 1

It was shown that the concepts of fixed points and manifolds can be defined for systems influenced by Gaussian noise. The fixed point in fact appears to remain unchanged when noise is added. This is quite a remarkable result, as it indicates that no matter what the noise level is, one will always be controlling to the same location. In this case it is noteworthy that the noise that was added in all experiments was symmetrical. It is possible that the fixed point may shift when asymmetrical noise is added.

Contrary to the fixed point, the manifold structure does appear to be influenced by noise. It appears that noise fuzzes out the directions that are associated with the noise free system. As noise becomes more dominant, the stable and unstable directions become less pronounced, and the system becomes dominated by statistical averages. As such, it follows that control based on the manifold structure will become less and less effective as noise levels increase.

There were also studies done investigating the effect of noise on the directions of maximum and minimum contraction near the fixed point. These directions appeared to not be affected by noise.

## 5.2 Concerning Conjecture 2

The control experiments showed that the boundaries of the theoretical stable control region remain intact as noise is added to the system. That is, the area of best control for the noisy system always stays within the noise free boundaries, even though the area shrinks with increased noise levels. It is of importance that the shrinking is not uniform relative to the edges of the theoretical region.

In each of the experiments it was apparent that the lowest part of the "control valley" tended to shift towards the theoretical edge closest to the origin of the control vector plane. In the limit to no noise, the valley minimum appeared towards that control vector that projects the system directly onto the fixed point.

The alteration to the original OGY method is then that a control vector is to be selected depending on the noise level. The above observations lead to the guidelines presented in section 4.3. These guidelines aim to optimize the search for the best control vector.

## 5.3 Concerning Conjecture 3

The guidelines developed were tested on two realistic model systems, the engine model and the CSTR model. The results from the engine model appear to support the guidelines, though a large number of data points was necessary to make the estimates converge. The results from the CSTR model are less conclusive, though they certainly do not contradict the guidelines given. Most likely the lack of sufficient data points causes estimation errors in the optimization. Unfortunately, gathering of a greater number of data points was prohibited by time constraints. Overall, evidence weighs in favor of the guidelines.

## 5.4 Overall objective and further study

The original OGY control method was modified by choosing a different control vector than was originally prescribed. The basic mechanics of the control algorithm remain unchanged. The control still requires only one vector multiplication per system cycle. Overall, the objective of the research has been achieved. However, a number of issues of interest for further study can be listed.

During the optimization of the control no consideration was given for the cost of control. That is, it might be possible that the optimal control as defined in the research is not optimal in the sense of minimal perturbations. If perturbations are expensive in an industrial environment, it is possible that a different cost minimizing function is desired. This would be greatly dependent on the particular system that is being studied, though it is conceivable that a general cost function could be derived.

All noise added to the systems in this research has been Gaussian. It would be of interest to study the effect of other noise distributions. In particular the effects of asymmetric distributions could be important, as these might shift the fixed point. This could conceivably results in the need of a totally different approach to optimizing control.

The guidelines developed in this research were derived more or less heuristicly. Confidence in these methods would be greatly improved if a more rigorous mathematical derivation of the presented concepts could be made.

Conversely, all experiments done here were computer simulations. Testing of these methods on actual physical systems is desirable. Other issues would also come into play in a physical experiment, such as how to deliberately add specific noise levels to real systems.

The systems used in this research have mostly been systems that did not need any embedding (the engine model uses a return map). The research has not accounted for the issues that arise from the embedding of time series. Dressler and Nitsche (1992) extended the original OGY method for use with embedded systems. Other researchers (e.g., Rhode, Rollins, Markworth, Edwards, Nguyen, Daw, and Thomas (1995)) have then argued that controlling directly to the fixed point is not the optimal control, as the system is also dependent on previous perturbations. How this is affected by dynamic noise is a relevant issue, since most real systems will most likely be embedded.

# Bibliography

# Bibliography


Christini, D. J. and J. Collins (1995, dec). Using noise and chaos control to control nonchaotic systems. *Physical Review E 52*(6), 5806–5809.

Collins, J., C. C. Chow, and T. T. Imhoff (1995, oct). Aperiodic stochastic resonance in excitable systems. *Physical Review E 52*(4), R3321–R3324.

Daw, C., C. Finney, J. Green, M. Kennel, J. Thomas, and F. Connolly (1996). A simple model for cyclic variations in a spark-ignition engine. Technical Report 962086, Society for Automotive Engineers.

Ding, M., E. Ott, and C. Grebogi (1994). Controlling chaos in a temporally irregular environment. *Physica D 74*, 386–394.

Dressler, U. and G. Nitsche (1992, jan). Controlling chaos using time delay coordinates. *Physical Review Letters 68*(1), 1–4.

Fahy, S. and D. Hamann (1992, aug). Transition from chaotic to nonchaotic behavior in randomly driven systems. *Physical Review Letters 69*(5), 761–764.

Hamm, A., T. Tél, and R. Graham (1994, feb). Noise-induced attractor explosions near tangent bifurcations. *Physics Letters A 185*, 313–320.

Herzel, H. (1988). Stabilization of chaotic orbits by random noise. *Z. angew. Math. Mech. 68*(11), 582–583.

Ikeda, K. (1979). Multiple-valued stationary state and its instability of the transmitted light by a ring cavity system. *Optics Communications 30*(1), 257–261.

In, V., W. L. Ditto, and M. L. Spano (1995, apr). Adaptive control and tracking of chaos in a magnetoelastic ribbon. *Physical Review E 51*(4), R2689–R2692.

Jorgensen, D. V. and R. Aris (1983). On the dynamics of a stirred tank with consecutive reactions. *Chemical Engineering Science 38*(1), 45–53.

Kapitaniak, T. (1996). *Controlling Chaos.* Academic Press.

Lorenz, E. N. (1963). Deterministic non-periodic flow. *Journal of Atmospheric Science 20*, 130.

Matsumoto, K. and I. Tsuda (1983). Noise-induced order. *Journal of Statistical Physics 31*(1), 87–106.

Mayer-Kress, G. and H. Haken (1981). The influence of noise on the logistic model. *Journal of Statistical Physics 26*(1), 149–171.

Neufelt, V. (Ed.) (1994). *Webster's New World Dictionary* (3 ed.). Prentice Hall/Macmillan.

Ott, E. (1993). *Chaos in Dynamical Systems.* Cambridge University Press.

Ott, E., C. Grebogi, and J. A. Yorke (1990, mar). Controlling chaos. *Physical Review Letters 64*(11), 1196–1199. The original.

Parmananda, P., P. Shepard, R. W. Rollins, and H. Dewald (1993, may). Control of chaos in an electrochemical cell. *Physical Review E 47*(5), R3003–R3006.

Poincaré, H. (1921). *The Foundation of Science: Science and Method.* New York: The Science Press.

Press, W. H., S. A. Teukolsky, W. T. Vetterling, and B. P. Flannery (Eds.) (1992). *Numerical Recipes in C.* Cambridge University Press.

Rajasekar, S. (1995, jan). Controlling of chaotic motion by chaos and noise signals in a logistic map and a Bonhoeffer-van der Pol oscillator. *Physical Review E 51*(1), 775–778.

Rhode, M., R. Rollins, A. Markworth, K. Edwards, K. Nguyen, C. Daw, and J. Thomas (1995, aug). Controlling chaos in a model of thermal pulse combustion. *Journal of Applied Physics 78*(4), 2224–2232.

Romeiras, F., C. Grebogi, E. Ott, and W. Dayawansa (1992). Controlling chaotic dynamical systems. *Physica D 58*(165), 165–192.

Sauer, T., J. A. Yorke, and M. Casdagli (1991). Embedology. *Journal of Satistical Physics 65*(3/4), 579–616.

Singer, J., Y.-Z. Wang, and H. H. Bau (1991). Controlling a chaotic system. *Physical Review Letters 66*(9), 1123–1125.

Strogatz, S. H. (1994). *Nonlinear Dynamics and Chaos.* Addison-Wesley Publishing Company.

Wackerbauer, R. (1995, nov). Noise-induced stabilization of the lorenz system. *Physical Review E 52*(5), 4745–4749.

# Appendix

# Appendix: Nomenclature

## General nomenclature

$\alpha =$ angle

$\lambda =$ Lyapunov exponent

$\lambda =$ eigenvalue

$\xi =$ noise

$\mathbf{b} =$ parameter Jacobian $\dfrac{d\mathbf{F}}{dp}$

$\mathbf{c} =$ control vector

$\mathbf{c}_o =$ control to fixed point vector

$\mathbf{c}_e =$ control vector located just inside the theoretical control region on the $\mathbf{c}_o$ – origin line

$\mathbf{F} =$ system function

$\mathbf{f} =$ left eigenvector

$\mathbf{J} =$ Jacobian $\dfrac{d\mathbf{F}}{d\mathbf{x}}$

$\mathbf{p} =$ parameter vector

$p_0 =$ nominal parameter value

$r =$ Euclidean distance in phase space between system states

$\mathbf{v} =$ eigenvector

$\mathbf{x} =$ system state

# Nomenclature for the CSTR model

## Variables and parameters

$$A_1, A_2 = \text{frequency factors}$$
$$A_c = \text{cooling surface area}$$
$$c_A, c_B = \text{reactant concentrations}$$
$$c_{Af} = \text{feed concentration}$$
$$E_1, E_2 = \text{activation energies}$$
$$\Delta H_1, \Delta H_2 = \text{reaction enthalpies}$$
$$q = \text{flowrate}$$
$$R = \text{gas constant}$$
$$T = \text{temperature}$$
$$T_c = \text{coolant temperature}$$
$$T_f = \text{feed temperature}$$
$$t' = \text{time}$$
$$V = \text{reactor volume}$$

## Dimensionless variables

$$t = \frac{qt'}{V}$$
$$u = \frac{c_A}{c_{Af}}$$
$$v = \frac{c_B}{c_{Af}}$$
$$w = \frac{E_1}{R\bar{T}^2}(T - \bar{T}), \bar{T} = \frac{T_f + \kappa T_c}{1 + \kappa}$$

## Dimensionless numbers

$$\alpha = \frac{VA_1}{q} e^{-\frac{E_1}{R\bar{T}}} \quad \text{(Damköhler number)}$$

$$\beta = -\Delta H_1 \frac{c_{Af}}{\rho c_p} \frac{E_1}{R\bar{T}^2} \quad \text{(dimensionless heat of reaction)}$$

$$h = \frac{\Delta H_1}{\Delta H_2}$$

$$\kappa = \frac{UA_c}{q \rho c_p} \quad \text{(dimensionless cooling rate)}$$

$$\sigma = \frac{A_2}{A_1} e^{\frac{E_1 - E_2}{R\bar{T}}}$$

# Vita

Nicolaas Aaldert van Goor was born in Jerusalem on July 31, 1968. There he attended Arabic and French schools before moving to the Netherlands in 1978. He graduated from the Revius Lyceum in Doorn in 1986, after which he entered the Delft University of Technology. During his studies at Delft, he was able to do internships in Buenos Aires, Argentina, as well as, Oak Ridge, Tennessee, U.S.A. He received his MS in Chemical Engineering from the Delft University of Technology in 1992. Following his graduation, Nicolaas entered the Doctoral program in Chemical Engineering at the University of Tennessee. The Doctoral degree was awarded in August, 1998.